H_2SO_4-H_2O-NH_3 ternary ion-mediated nucleation (TIMN): Kinetic-based model and comparison with CLOUD measurements

Fangqun Yu[1], Alexey B. Nadykto[1, 2], Jason Herb[1], Gan Luo[1], Kirill M. Nazarenko[2], and Lyudmila A. Uvarova[2]

Correspondence to: F. Yu (fyu@albany.edu)

[1] Atmospheric Sciences Research Center, University at Albany, Albany, New York, US

[2] Department of Applied Mathematics, Moscow State Univ. of Technology "Stankin", Russia

Abstract. New particle formation (NPF) is known to be an important source of atmospheric particles that impacts air quality, hydrological cycle, and climate. Although laboratory measurements indicate that ammonia enhances NPF, the physico-chemical processes underlying the observed effect of ammonia on NPF are yet to be understood. Here we present a comprehensive kinetically-based H_2SO_4-H_2O-NH_3 ternary ion-mediated nucleation (TIMN) model that is based on the thermodynamic data derived from both quantum-chemical calculations and laboratory measurements. NH_3 was found to reduce nucleation barriers for neutral, positively charged, and negatively charged clusters differently, due to large differences in the binding strength of NH_3, H_2O, and H_2SO_4 to small clusters of different charging states. The model reveals the general favor of nucleation of negative ions, followed by nucleation on positive ions and neutral nucleation, for which higher NH_3 concentrations are needed, in excellent agreement with Cosmics Leaving OUtdoor Droplets (CLOUD) measurements. The TIMN model explicitly resolves dependences of nucleation rates on all the key controlling parameters, and captures well the absolute values of nucleation rates as well as the dependence of TIMN rates on concentrations of NH_3 and H_2SO_4, ionization rates, temperature, and relative humidity observed in the well-controlled CLOUD measurements. The kinetic model offers physico-chemical insights into the ternary nucleation process and provides a physics-based approach to calculate TIMN rates under a wide range of atmospheric conditions.

1. Introduction

New particle formation (NPF), an important source of particles in the atmosphere, is a dynamic process involving interactions among precursor gas molecules, small clusters, and pre-existing particles (Yu and Turco, 2001; Zhang et al., 2012). H_2SO_4 and H_2O are known to play an important role in atmospheric particle formation (e.g., Doyle, 1961). In typical atmospheric conditions, the species dominating the formation and growth of small clusters is H_2SO_4. The contribution of H_2O to the nucleation is related to the hydration of H_2SO_4 clusters (or, in the other words, modification of the composition of nucleating clusters) that reduces the H_2SO_4 vapor pressure and hence diminishes the evaporation of H_2SO_4 from the pre-nucleation clusters. NH_3, the most abundant gas-phase base molecule in the atmosphere and a very efficient neutralizer of sulfuric acid solutions, has long been proposed to enhance nucleation in the lower troposphere (Coffman and Hegg, 1995) although it has been well recognized that earlier versions of classical ternary nucleation model (Coffman and Hegg, 1995; Korhonen et al., 1999; Napari et al., 2002) significantly over-predict the effect of ammonia (Yu, 2006a; Merikanto et al., 2007; Zhang et al., 2010).

The impacts of NH_3 on NPF have been investigated in a number of laboratory studies (Kim et al., 1998; Ball et al., 1999; Hanson and Eisele, 2002; Benson et al., 2009; Kirkby et al., 2011; Zollner et al., 2012; Froyd and Lovejoy, 2012; Glasoe et al., 2015; Schobesberger et al., 2015; Kurten et al., 2016) including those recently conducted at the European Organization for Nuclear Research (CERN) in the framework of the CLOUD (Cosmics Leaving OUtdoor Droplets) experiment that has provided a unique dataset for quantitatively examining the dependences of ternary H_2SO_4-H_2O-NH_3 nucleation rates on concentrations of NH_3 ($[NH_3]$) and H_2SO_4 ($[H_2SO_4]$), ionization rate (Q), temperature (T), and relative humidity (RH) (Kirkby et al., 2011; Kurten et al., 2016). The experimental conditions in the CLOUD chamber, a 26.1 m^3 stainless steel cylinder, were well controlled, while impacts of potential contaminants were minimized (Schnitzhofer et al., 2014; Duplissy et al., 2016). Based on CLOUD measurements in H_2SO_4-H_2O-NH_3 vapor mixtures, Kirkby et al. (2011) reported that an increase of $[NH_3]$ from ~ 0.03 ppb (parts per billion, by volume) to ~ 0.2 ppb can enhance ion-mediated (or induced) nucleation rate by 2-3 orders of magnitude and that the ion-mediated nucleation rate is a factor of 2 to >10 higher than that of neutral nucleation under typical level of contamination by amines. In the presence of ionization, highly polar common atmospheric nucleation precursors such as H_2SO_4, H_2O, and NH_3 molecules tend to cluster around ions; and charged clusters are generally much more stable than their neutral counterparts with enhanced growth rates as a result of dipole-charge interactions (Yu and Turco, 2001).

Despite of various laboratory measurements indicating that ammonia enhances NPF, the physico-chemical processes underlying the observed different effects of ammonia on the formation of neutral, positively charged and negatively charged clusters (Schobesberger et al., 2015) are yet to be understood. To achieve such an understanding, a nucleation model based on the first principles is needed. Such a model is also necessary to extrapolate data obtained in a limited number of experimental conditions to a wide range of atmospheric conditions, where [NH_3], [H_2SO_4], ionization rates, T, RH and surface areas of preexisting particles vary widely depending on the region, pollution level and season. The present work aims to address these issues by developing a kinetically-based H_2SO_4-H_2O-NH_3 ternary ion-mediated nucleation (TIMN) model that is based on the molecular clustering thermodynamic data. The model predictions are compared with relevant CLOUD measurements and previous studies.

2. Kinetic-based H_2SO_4-H_2O-NH_3 ternary ion-mediated nucleation (TIMN) model

2.1. Background

Most nucleation models developed in the past for H_2SO_4-H_2O binary homogeneous nucleation (e.g., Vehkamäki et al., 2002), H_2SO_4-H_2O ion-induced nucleation (e.g., Hamill et al., 1982; Raes et al., 1986; Laakso et al., 2003), and H_2SO_4-H_2O-NH_3 ternary homogeneous nucleation (Coffman and Hegg, 1995; Korhonen et al., 1999; Napari et al., 2002) have been based on the classical approach, which employs capillarity approximation (i.e., assuming that small clusters have same properties as bulk) and calculate nucleation rates according to the free energy change associated with the formation of a "critical embryo". Yu and Turco (1997, 2000, 2001) developed a neutral and charged binary H_2SO_4-H_2O nucleation model using a kinetic approach that explicitly treats the complex interactions among small air ions, neutral and charged clusters of various sizes, precursor vapor molecules, and pre-existing aerosols. The formation and evolution of cluster size distributions for positively and negatively charged cluster ions and neutral clusters affected by ionization, recombination, neutralization, condensation, evaporation, coagulation, and scavenging, has been named as ion-mediated nucleation (IMN) (Yu and Turco, 2000). The IMN theory significantly differs from classical ion-induced nucleation (IIN) theory (e.g., Hamill et al., 1982; Raes et al., 1986; Laakso et al., 2003) which is based on a simple modification of the free energy for the formation of a "critical embryo" by including the electrostatic potential energy induced by the embedded charge (i.e., Thomson effect (Thomson, 1888)). The classical approach does not properly account for the kinetic limitation to embryo development, enhanced stability and growth of charged clusters associated with dipole-charge interaction (Nadykto and Yu, 2003; Yu, 2005), and the important contribution of neutral clusters resulting from ion-ion recombination to nucleation (Yu and Turco, 2011). In contrast, these important physical processes are explicitly considered in the kinetic-based IMN model (Yu, 2006b).

Since the beginning of the century, nucleation models based on kinetic approach have also been developed in a number of research groups (Lovejoy et al., 2004; Sorokin et al., 2006; Chen et al., 2012; Dawson et al., 2012; McGrath et al., 2012). Lovejoy et al. (2004) developed a kinetic ion nucleation model, which explicitly treats the evaporation of small neutral and negatively charged H_2SO_4-H_2O clusters. The thermodynamic data used in their model were obtained from measurements of small ion clusters, ab initio calculations, thermodynamic cycle, and some approximations (adjustment of Gibbs free energy for neutral clusters calculated based on liquid droplet model, interpolation, etc.). Lovejoy et al. (2004) did not consider the nucleation on positive ions. Sorokin et al. (2006) developed an ion-cluster-aerosol kinetic (ICAK) model which uses the thermodynamic data reported in Froyd and Lovejoy (2003a, b) and empirical correction terms proposed by Lovejoy et al. (2004). Sorokin et al. (2006) used the ICAK model to simulate dynamics of neutral and charged H_2SO_4-H_2O cluster formation and compared the modeling results with their laboratory measurements. Chen et al. (2012) developed an approach for modeling new particle formation based on a sequence of acid-base reactions, with sulfuric acid evaporation rates (from clusters) estimated empirically based on measurements of neutral molecular clusters taken in Mexico City and Atlanta. Dawson et al. (2012) presented a semi-empirical kinetics model for nucleation of methanesulfonic acid (MSA), amines, and water that explicitly accounted for the sequence of reactions leading to formation of stable particles. The kinetic models of Chen et al. (2012) and Dawson et al. (2012) consider only neutral clusters.

McGrath et al. (2012) developed the Atmospheric Cluster Dynamics Code (ACDC) to model the cluster kinetics by solving the birth–death equations explicitly, with evaporation rate coefficients derived from formation free energies calculated by quantum chemical methods (Almeida et al., 2013; Olenius et al., 2013). The ACDC model applied to the H_2SO_4-dimethylamine (DMA) system considers 0–4 base molecules and 0–4 sulfuric acid molecules (Almeida et al., 2013). Olenius et al. (2013) applied the ACDC model to simulate the steady-state concentrations and kinetics of neutral, and negatively and positively charged clusters containing up to 5 H_2SO_4 and 5 NH_3 molecules. In ACDC, the nucleation rate is calculated as the rate of clusters growing larger than the upper bounds of the simulated system (i.e., clusters containing 4 or 5 H_2SO_4 molecules) (Kurten et al., 2016).

The kinetic IMN model developed by Yu and Turco (1997, 2001) explicitly simulates the dynamics of neutral, positively charged, and negatively charged clusters, based on a discrete-sectional bin structure that covers the clusters containing 0, 1, 2, …, 15, … H_2SO_4 molecules to particles containing thousands of H_2SO_4 (and H_2O) molecules. In the first version of the kinetic IMN model (Yu and Turco, 1997, 2001), due to the lack of thermodynamic data for the small clusters, the compositions of neutral and charged clusters were assumed to be the same and the evaporation of small clusters was accounted for using a simple adjustment to the condensation

accommodation coefficients. Yu (2006b) developed a second-generation IMN model which incorporated newer thermodynamic data (Froyd, 2002; Wilhelm et al., 2004) and physical algorithms (Froyd, 2002; Wilhelm et al., 2004) and explicitly treated the evaporation of neutral and charged clusters. Yu (2007) further improved the IMN model by using two independent measurements (Marti et al., 1997; Hanson and Eisele, 2000) to constrain monomer hydration in the H_2SO_4-H_2O system and by incorporating experimentally determined energetics of small neutral H_2SO_4-H_2O clusters that became available then (Hanson and Lovejoy, 2006; Kazil et al., 2007). The first and second generations of the IMN model were developed for the H_2SO_4-H_2O binary system, although the possible effects of ternary species such as the impact of NH_3 on the stability of both neutral and charged pre-nucleation clusters have been pointed out in these previous studies (Yu and Turco, 2001; Yu, 2006b). The present work extends the previous versions of the IMN model in binary H_2SO_4-H_2O system to ternary H_2SO_4-H_2O-NH_3 system, as described below.

2.2. Model representation of kinetic ternary nucleation processes

Figure 1 schematically illustrates the evolution of charged and neutral clusters/droplets explicitly simulated in the kinetic H_2SO_4-H_2O-NH_3 TIMN model. Here, H_2SO_4 (S) is the key atmospheric nucleation precursor driving the TIMN process while ions, H_2O (W), and NH_3 (A) stabilize the H_2SO_4 clusters and enhance in this way H_2SO_4 nucleation rates. Ions also enhance cluster formation rates due to the interaction with polar nucleating species leading to enhanced collision cross sections (Nadykto and Yu, 2003). The airborne ions are generated by galactic cosmic rays (GCRs) or produced by radioactive emanations, lightning, corona discharge, combustion and other ionization sources. The initial negative ions, which are normally assumed to be NO_3^-, are converted into HSO_4^- core ions (i.e., S^-) and, then, to larger H_2SO_4 clusters in the presence of gaseous H_2SO_4. The initial positive ions H^+W_w are converted into $H^+A_{1-2}W_w$ in the presence of NH_3, $H^+S_sW_w$ in the presence of H_2SO_4, or $H^+A_aS_sW_w$ in the case, when both NH_3 and H_2SO_4 are present in the nucleating vapors. Some of the binary H_2SO_4-H_2O clusters, both neutral and charged, transform into ternary ones by taking up NH_3 vapors. The molar fraction of ternary clusters in nucleating vapors depends on [NH_3], the binding strength of NH_3 to binary and ternary pre-nucleation clusters, cluster composition, and ambient conditions such as T and RH.

Similar to the kinetic binary IMN (BIMN) model (Yu, 2006b), the kinetic TIMN model employs a discrete-sectional bin structure to represent clusters/particles. The bin index i represent the amount of core component (i.e., H_2SO_4). For small clusters ($i \le i_d = 30$ in this study), i is the

number of H_2SO_4 molecules in the cluster (i.e., $i = s$) and the core volume of i^{th} bin $v_i = i \times v_1$, where v_1 is the volume of one H_2SO_4 molecule. When $i > i_d$, $v_i = VRAT_i \times v_{i-1}$, where $VRAT_i$ is the volume ratio of i^{th} bin to $(i\text{-}1)^{th}$ bin. The discrete-sectional bin structure enables the model to cover a wide range of sizes of nucleating clusters/particles with the highest possible size resolution for small clusters (Yu, 2006b). For clusters with a given bin i, the associated amounts of water and NH_3 and thus the effective radius of each ternary cluster are calculated based on the equilibrium of clusters/particles with the water vapor and/or ammonia, as described in later sections.

The evolution of positive, negative, and neutral clusters due to the simultaneous condensation, evaporation, recombination, coagulation, and other loss processes, is described by the following differential equations obtained by the modification of those describing for the evolution of binary H_2SO_4-H_2O system (Yu, 2006b):

$$\frac{\partial N_0^+}{\partial t} = Q + \gamma_1^+ N_1^+ - N_0^+ \left(\sum_{j=1}^{i_{\max}} \beta_{i,j}^+ N_j^0 + \sum_{j=0}^{i_{\max}} \eta_{i,j}^+ N_j^+ + \sum_{j=0}^{i_{\max}} \alpha_{0,j}^{+,-} N_j^- \right) - N_0^+ L_0^+ \tag{1}$$

$$\frac{\partial N_0^-}{\partial t} = Q + \gamma_1^- N_1^- - N_0^- \left(\sum_{j=1}^{i_{\max}} \beta_{i,j}^- N_j^0 + \sum_{j=0}^{i_{\max}} \eta_{i,j}^- N_j^- + \sum_{j=0}^{i_{\max}} \alpha_{0,j}^{-,+} N_j^+ \right) - N_0^- L_0^- \tag{2}$$

$$\begin{aligned} \frac{\partial N_1^0}{\partial t} &= P_{\mathrm{H2SO4}} + \sum_{j=2}^{i_{\max}} \delta_{j,2}\, \gamma_j^0\, N_j^0 + \sum_{j=1}^{i_{\max}} (\gamma_j^+\, N_j^+ + \gamma_j^-\, N_j^-) \\ &\quad - N_1^0 \left(\sum_{j=1}^{i_{\max}} (1 - f_{1,j,1}) \beta_{1,j}^0 N_j^0 + \sum_{j=0}^{i_{\max}} (\beta_{j,1}^+ N_j^+ + \beta_{j,1}^- N_j^-) \right) - N_1^0 L_1^0 \end{aligned} \tag{3}$$

$$\begin{aligned} \frac{\partial N_i^+ (i \ge 1)}{\partial t} &= g_{i+1,i}\, \gamma_{i+1}^+\, N_{i+1}^+ - g_{i,i-1}\, \gamma_i^+\, N_i^+ + \sum_{j=0}^{i-1} \sum_{k=1}^{i} \frac{v_j}{v_i} f_{j,k,i} \beta_{j,k}^+ N_j^+ N_k^0 + \sum_{j=0}^{i-1} \sum_{k=0}^{i} \frac{v_j}{v_i} f_{j,k,i} \eta_{j,k}^+ N_j^+ N_k^+ \\ &\quad + \sum_{j=0}^{i} \sum_{k=1}^{i} \frac{v_k}{v_i} f_{j,k,i} \beta_{j,k}^+ N_j^+ N_k^0 - N_i^+ \left(\sum_{j=1}^{i_{\max}} (1 - f_{i,j,i}) \beta_{i,j}^+ N_j^0 + \sum_{j=0}^{i_{\max}} (1 - f_{i,j,i}) \eta_{i,j}^+ N_j^+ + \sum_{j=0}^{i_{\max}} \alpha_{i,j}^{+,-} N_j^- \right) - N_i^+ L_i^+ \end{aligned} \tag{4}$$

$$\begin{aligned} \frac{\partial N_i^- (i \ge 1)}{\partial t} &= g_{i+1,i}\, \gamma_{i+1}^-\, N_{i+1}^- - g_{i,i-1}\, \gamma_i^-\, N_i^- + \sum_{j=0}^{i-1} \sum_{k=1}^{i} \frac{v_j}{v_i} f_{j,k,i} \beta_{j,k}^- N_j^- N_k^0 + \sum_{j=0}^{i-1} \sum_{k=0}^{i} \frac{v_j}{v_i} f_{j,k,i} \eta_{j,k}^- N_j^- N_k^- \\ &\quad + \sum_{j=0}^{i} \sum_{k=1}^{i} \frac{v_k}{v_i} f_{j,k,i} \beta_{j,k}^- N_j^- N_k^0 - N_i^- \left(\sum_{j=1}^{i_{\max}} (1 - f_{i,j,i}) \beta_{i,j}^- N_j^0 + \sum_{j=0}^{i_{\max}} (1 - f_{i,j,i}) \eta_{i,j}^- N_j^- + \sum_{j=0}^{i_{\max}} \alpha_{i,j}^{-,+} N_j^+ \right) - N_i^- L_i^- \end{aligned} \tag{5}$$

$$\begin{aligned} \frac{\partial N_i^0 (i \ge 2)}{\partial t} &= g_{i+1,i}\, \gamma_{i+1}^0 N_{i+1}^0 - g_{i,i-1}\, \gamma_i^0\, N_i^0 + \sum_{j=1}^{i} \sum_{k=1}^{i-1} \frac{v_k}{v_i} f_{j,k,i} \beta_{j,k}^0 N_j^0 N_k^0 \\ &\quad + \sum_{j=0}^{i} \sum_{k=0}^{i} f_{j,k,i} \alpha_{j,k}^{+,-} \left(\frac{v_k}{v_i} N_j^+ N_k^- + \frac{v_j}{v_i} N_j^+ N_k^- \right) - N_i^0 \left(\sum_{j=1}^{i_{\max}} (1 - f_{i,j,i}) \beta_{i,j}^0 N_j^0 + \sum_{j=0}^{i_{\max}} (\beta_{j,i}^+ N_j^+ + \beta_{j,i}^- N_j^-) \right) - N_i^0 L_i^0 \end{aligned} \tag{6}$$

In Eqs. (1-6), the superscripts "+", "-", and "0" refer to positive, negative, and neutral clusters, respectively, while subscripts *i, j, k* represent the bin indexes. $N_0^{+,-}$ and Q are the concentration of initial ions not containing H_2SO_4 (i.e., $H^+A_aW_w$ and NO_3^-) and the ionization rate, respectively. N_i is the total number concentration (cm^{-3}) of all cluster/particles (binary + ternary) in the bin *i*. For small clusters ($i \le i_d$), N_i is the number concentration (cm^{-3}) of all clusters containing *i* H_2SO_4 molecules. For example, N_1^0 is the total concentration of binary and ternary neutral clusters containing one H_2SO_4 molecules. P_{H2SO4} is the gas-phase production rate of neutral H_2SO_4 molecules. $L_i^{+,-,0}$ is the loss rate due to scavenging by pre-existing particles, and wall and dilution losses in the laboratory chamber studies (Kirkby et al., 2011; Olenius et al., 2013; Kurten et al., 2016). $f_{j,k,i}$ is the volume fraction of intermediate particles (volume = $v_j + v_k$) partitioned into bin *i* with respect to the core component – H_2SO_4, as defined in Jacobson et al. (1994). $g_{i+1,i} = v_1/(v_{i+1} - v_i)$ is the volume fraction of intermediate particles of volume (v_{i+1} - v_1) partitioned into bin *i*. $\delta_{j,2}$=2 at *j*=2 and $\delta_{j,2}$ =1 at *j*≠2. γ_i^+, γ_i^-, and γ_i^0 are the mean (or effective) cluster evaporation coefficients for positive, negative and neutral clusters in bin *i*, respectively. $\beta_{i,j}^+$, $\beta_{i,j}^-$, $\beta_{i,j}^0$ are the coagulation kernels for the neutral clusters/particles in bin *j* interacting with positive, negative, and neutral clusters/particles in bin *i*, respectively, which reduce to the condensation coefficients for H_2SO_4 monomers at *j*=1. $\eta_{j,k}^+$ and $\eta_{j,k}^-$ are coagulation kernels for clusters/particles of like sign from bin *j* and clusters/particles from bin *k*. $\alpha_{i,j}^{+,-}$ is the recombination coefficient for positive clusters/particles in bin *i* interacting with negative clusters/particles in bin *j*, while $\alpha_{i,j}^{-,+}$ is the recombination coefficient negative clusters/particles from bin *i* interacting with positively charged clusters/particles from bin *j*.

The methods for calculating *β, γ, η,* and *α* for binary H_2SO_4-H_2O clusters have been described in our previous publications (Yu and Turco, 2001; Nadykto and Yu, 2003; Yu, 2006b). Dipole-charge interaction (Nadykto and Yu, 2003), image capture and three-body trapping effects (Hoppel and Frick, 1986) are considered in the calculation of these coefficients. Since *β, η,* and *α* depend on the cluster mass (or size) rather than on the cluster composition, schemes for calculating these properties in binary and ternary clusters are identical. In contrast, *γ* is quite sensitive to cluster

composition. The evaporation rate coefficient of H_2SO_4 molecules from clusters containing *i* H_2SO_4 molecules (γ_i) is largely controlled by the stepwise Gibbs free energy change $\Delta G_{i-1,i}$ of formation of an *i*-mer from an (*i*-1)-mer (Yu, 2007)

$$\gamma_i = \beta_{i-1} N^{o} \exp\left(\frac{\Delta G_{i-1,i}}{RT}\right) \quad (7)$$

$$\Delta G_{k-1,k} = -RTln\left(\frac{N_1^0}{N^o}\right) + \Delta H^{o}_{k-1,k} - T\Delta S^{o}_{k-1,k} \quad (8)$$

where *R* is the molar gas constant, N^{o} is the number concentration of H_2SO_4 at a given T under the reference vapor pressure P of 1 atm. ΔH^{o} and ΔS^{o} are enthalpy and entropy changes under the standard conditions (T=298 K, P=1 atm), respectively. The temperature dependence of ΔH^{o} and ΔS^{o}, which is generally small and typically negligible over the temperature range of interest (Nadykto et al., 2009), was not considered.

2.3. Thermochemical data of neutral and charged binary and ternary clusters

ΔH, ΔS and ΔG values needed to calculate cluster evaporation rates (Eq. 7) for the TIMN model can be derived from laboratory measurements and computational quantum chemistry (QC) calculation. Thermochemical properties of neutral and charged binary and ternary clusters obtained using the computational chemical methods and comparisons of computed energies with available experimental data and semi-experimental estimates are given in Tables A1-A4 and discussed in Appendix. As an example, Figure 2 shows ΔG associated with the addition of water (ΔG^{o}_{+W}), ammonia (ΔG^{o}_{+A}), and sulfuric acid (ΔG^{o}_{+S}) to binary and ternary clusters as a function of the cluster hydration number *w*. H_2O has high proton affinity and, thus, H_2O is strongly bonded to all positive ions with low *w*. ΔG^{o}_{+W} expectedly becomes less negative and binding of H_2O to binary and ternary clusters weakens due to the screening effect as the hydration number *w* is growing (Fig. 2a). The presence of NH_3 in the clusters weakens binding of H_2O to positive ions. For example, ΔG^{o}_{+W} for $H^+A_1W_wS_1$ is ~3-4 kcal mol^{-1} less negative than that for $H^+W_wS_1$ at *w*=3-6. The addition of one more NH_3 to the clusters to form $H^+A_2W_w$ and $H^+A_2W_wS_1$ further weakens H_2O binding by ~1.5-6 kcal mol^{-1} at *w*=1-3, while exhibiting much smaller impact on hydration free energies at *w*>3. Both the absolute values and trends in ΔG^{o}_{+W} derived from calculations are in agreement with the laboratory measurements within the uncertainty range of ~1-2 kcal mol^{-1} for

both QC calculations and measurements. This confirms the efficiency and precision of QC methods in calculating thermodynamic data needed for the development of nucleation models.

The proton affinity of NH_3 is 204.1 kcal mol^{-1}, which is 37.5 kcal mol^{-1} higher than that of H_2O (166.6 kcal mol^{-1}) (Jolly, 1991). The hydrated hydronium ions (H^+W_w) are easily converted to $H^+A_1W_w$ in the presence of NH_3. The binding of NH_3 and H_2O molecule to H^+W_w exhibits a similar pattern. In particular, binding of NH_3 to H^+W_w decreases as w is growing, with ΔG^o_{+A} for $H^+A_1W_w$ ranging from -52.08 kcal mol^{-1} at w=1 to -8.32 kcal mol^{-1}at w = 9. The binding of NH_3 to $H^+W_wS_1$ ions is also quite strong, with ΔG^o_{+A} for $H^+A_1W_wS_1$ ranging from -33.14 kcal mol^{-1} at w=1 and to -10.57 kcal mol^{-1} at w=6. The addition of the NH_3 molecule to $H^+A_1W_w$ (to form $H^+A_2W_w$) is much less favorable thermodynamically than that to H^+W_w, with the corresponding ΔG^o_{+A} being -22 kcal mol^{-1} and -6 kcal mol^{-1} at w=2 and w=6, respectively. The ΔG^o_{+A} values for $H^+A_2W_w$ are 3-5 kcal mol^{-1} more negative than the experimental values at w=0-1; however, they are pretty close to experimental data at w=2-3 (Fig. 2b and Table A2). While it is possible that the QC method overestimates the charge effect on the formation free energies of smallest clusters, the possible overestimation at w=0-1 will not affect nucleation calculations because most of $H^+A_2W_w$ in the atmosphere contain more than 2 water molecules (i.e., w>2) due to the strong hydration (see Table A2 and Fig. 2a).

A comparison of QC and semi-experimental estimates of ΔG^o_{+S} values associated with the attachment of H_2SO_4 to positive ions shown in Fig. 2c indicates that computed ΔG^o_{+S} values agree well with observations for $H^+W_wS_1$ and $H^+A_1W_wS_1$ but differ by ~2-4 kcal mol^{-1} from semi-experimental values for $H^+A_2W_wS_1$. As seen from Figs. 2a and 2c, the attachment of NH_3 to $H^+W_wS_1$ weakens the binding of both H_2O and H_2SO_4 to the clusters. This suggests that the attachment of NH_3 leads to the evaporation of H_2SO_4 and H_2O molecules from the clusters. In other words, H_2SO_4 is less stable in $H^+A_1W_wS_1$ than in $H^+W_wS_1$ (Fig. 2c). While this may be taken for the indication that NH_3 inhibits nucleation on positive ions at the first look, further calculations show that binding of NH_3 to $H^+A_1W_wS_1$ is quite strong (Fig. 2b) and that H_2SO_4 in $H^+A_2W_wS_1$ cluster is much more stable than that in $H^+A_1W_wS_1$, with ΔG^o_{+S} being by ~7 kcal mol^{-1} more negative at w>2. The $H^+A_2W_wS_1$ cluster can also be formed via the attachment of H_2SO_4 to $H^+A_2W_w$. In the presence of sufficient concentrations of NH_3, a large fraction of positively charged H_2SO_4 monomers exist in the form of $H^+A_2W_wS_1$ and, hence, NH_3 enhances nucleation of positive ions. Since positively charged H_2SO_4 dimers are expected to contain large number of water molecules, we have not yet computed and derived quantum chemical data for these clusters. The CLOUD measurements do indicate that once $H^+A_2W_wS_1$ are formed, they can continue to grow to larger $H^+A_aW_wS_s$ clusters along a=s+1 pathway (Schobesberger et al., 2015).

Figure 2 shows clearly that the calculated values in most cases agree with measurements within the uncertainty range that justifies the application of QC values in the case, when no reliable experimental data are available.

2.4. Nucleation barriers for neutral/charged clusters and size-dependent evaporation rates

Nucleation barriers and cluster evaporation rates are critically important for calculations of nucleation rates. This section describes the methods employed to calculate the evaporation rates of nucleating clusters of variable sizes and compositions (i.e., γ in Eqs. 1-6) in the TIMN model.

2.4.1 Equilibrium distributions of small binary and ternary clusters

In the atmosphere, [H_2O] is much higher than [H_2SO_4] and, thus, H_2SO_4 clusters/particles are always in equilibrium with water vapor (Yu, 2007). In the lower troposphere, where most of the nucleation events were observed, [H_2SO_4] is typically at sub-ppt to ppt level, while [NH_3] is in the range of sub-ppb to ppb levels (Butler et al., 2016; Warner et al., 2016) (note that, in what follows, all references to vapor mixing ratios – parts per billion and parts per trillion – are by volume). This means that small ternary clusters can be considered to be in equilibrium with H_2O and NH_3 vapors. Like the previous BIMN model derived assuming equilibrium of binary clusters with water vapor, the present TIMN model treats small clusters containing a given number of H_2SO_4 molecules as being in equilibrium with both H_2O and NH_3. Their relative concentrations are calculated using the thermodynamic data shown in Tables A1-A4. It should be noted that the system may deviate from equilibrium if [NH_3] is less than or close to [H_2SO_4]. Under such cases, the equilibrium assumption may overestimate nucleation rates.

Figure 3 shows the relative abundance (or molar fractions) of small positive, negative, and neutral clusters ($f_{s,a,w}^{+,-,0}$) containing a given number of H_2SO_4 molecules at the ambient temperature of 292 K and three different combinations of RH and [NH_3] values. As a result of relative instability of H_2SO_4 in $H^+A_1W_wS_1$ compared to $H^+W_wS_1$ or $H^+A_2W_wS_1$ (Fig. 2c), most of positive ions with one H_2SO_4 molecule exist in the form of either as $H^+W_wS_1$ or $H^+A_2W_wS_1$ (i.e, containing either zero or two NH_3 molecules, Fig. 3a). When [NH_3]=0.3 ppb (with T=292 K), most of the positive ions containing one H_2SO_4 molecule do not contain NH_3 and their composition is dominated by $H^+W_wS_1$ ($\overline{w}$=~7). At the given T and [NH_3]=0.3 ppb, around 17% of positive ions with one H_2SO_4 molecule contain two NH_3 molecules at RH=38%. The fraction of positive ions containing one H_2SO_4 and two NH_3 molecules decreases to 0.9%, when RH = 90%. At T=292 K and RH=38%, the increase in [NH_3] by a factor of 10 to 3 ppb leads to the domination of $H^+A_2W_wS_1$ (~95%) in the composition of positively charged H_2SO_4 monomers. As expected, the composition of positive ions and their contribution to nucleation depends on T, RH, and [NH_3].

The incorporation of the quantum chemical and experimental clustering thermodynamics in the framework of the kinetic nucleation model enables us to study all these dependencies.

As a result of very weak binding of H_2O and NH_3 to small negative ions (Table A4), nearly all negatively charged clusters with s=0-1 do not contain water and ammonia (not shown). In the case, when *s* is growing to 2, all $S^-S_2A_aW_w$ clusters still do not contain NH_3 (i.e., a=0), while only 20-40% of them contain one water molecule (*w*=1) (Fig. 3b). As *s* further increases to 3, NH_3 begins to get into some of the negatively charged ions. The fraction of $S^-S_3A_aW_w$ clusters containing one NH_3 molecule is 9% at RH=38% and $[NH_3]$=0.3ppb, 3% at RH=90% and $[NH_3]$=0.3 ppb, and 50% at RH=38% and $[NH_3]$=3 ppb. Most of $S^-S_3W_w$ clusters are hydrated while the fraction of $S^-S_3A_aW_w$ clusters containing two NH_3 molecules at these ambient conditions is negligible. The fraction of negative cluster ions containing two NH_3 molecules becomes significant at *s*=4 (Fig. 3b) and increases from 28% at $[NH_3]$=0.3 ppb to 80% at $[NH_3]$=3 ppb at RH=38%. At $[NH_3]$ =0.3 ppb, the increase in RH from 38% to 90% reduces the fraction of NH_3 containing $S^-S_3A_aW_w$ clusters (i.e, *a*>=1) from to 95% to 70%, demonstrating a significant impact of RH on cluster compositions and emphasizing the importance of accounting for the RH in calculations of ternary nucleation rates.

The equilibrium distributions of neutral clusters are presented in Fig. 3c (H_2SO_4 monomers and dimers) and Fig. 3d (H_2SO_4 trimers and tetramers). Hydration is accounted for in the case of monomers and dimers and not included, due to lack of thermodynamic data, in calculations for trimers and tetramers. Based on the thermodynamic data shown in Table A3, the dominant fraction of neutral monomers is hydrated (79% at RH=38% and 94% at RH=90%) while the fraction of monomers containing NH_3 is negligible (0.02% at $[NH_3]$=0.3 ppb and 0.2% at $[NH_3]$=3 ppb, RH=38%). As a result of the growing binding strength of NH_3 with the cluster size (Table A3), the fraction of neutral sulfuric acid dimers containing one NH_3 molecule reaches 18% at $[NH_3]$=0.3 ppb and 69% at $[NH_3]$=3 ppb when T=292 K and RH=38%. In the case of H_2SO_4 trimers and tetramers, data shown in Figure3d are limited to the relative abundance of unhydrated clusters only. Under the given conditions, most of trimers contain two NH_3 molecules while most tetramers contain 3 NH_3 molecules. At $[NH_3]$=3 ppb, ~2% of trimers contain three NH_3 molecules (i.e., *s*=*a*=3) and 55% of tetramers contain four NH_3 molecules (i.e., *s*=*a*=4). As a result of a significant drop of ΔG^o_{+A} in the case, when *a*/*s* ratio exceeds one (Table A3), the fraction of neutral clusters with *a*=*s*+1 are negligible. The cluster distributions clearly indicate that small sulfuric acid clusters are still not fully neutralized by NH_3 even if $[NH_3]$ is at ppb level; and that the degree of neutralization (i.e., a:s ratio) increases with the cluster size.

2.4.2 Mean stepwise and accumulative Gibbs free energy change and impact of ammonia

In the TIMN model, the equilibrium distributions are used to calculate number concentrations weighted stepwise Gibbs free energy change for adding one H_2SO_4 molecule to form a neutral, positively charged, and negatively charged cluster containing s H_2SO_4 molecules ($\overline{\Delta G}_{s-1,s}$):

$$\overline{\Delta G}_{s-1,s}^{+,-,0} = \sum_{a,w} f_{s,a,w}^{+,-,0} \Delta G_{s-1,s,a,w}^{+,-,0} \quad (9)$$

where $f_{s,a,w}^{+,-,0}$ is the equilibrium fraction of a particular cluster within a cluster type as shown in Fig. 3.

In the atmosphere, where substantial nucleation is observed, the sizes of critical clusters are generally small (s < ~5–10) (e.g., Sipilä et al., 2010) and nucleation rates are largely controlled by the stability (or γ) of small clusters with s < ~5–10. QC calculations and experimental data on clustering thermodynamics available for clusters of small sizes (Tables A2–A4), are critically important as the formation of these small clusters is generally the limiting step for nucleation. Nevertheless, thermodynamics data for larger clusters are also needed to develop a robust nucleation model that can calculate nucleation rates under various conditions. Both measurements and QC calculations (Tables A2–A4) show significant effects of charge and charge signs (i.e., positive or negative) on the stability and composition of small clusters. These charge effects decrease quickly as the clusters grow, due to the short-ranged nature of dipole-charge interaction and the quick decrease of electrical field strength around charged clusters as cluster sizes increase (Yu, 2005). Based on experimental data (Kebarle et al., 1967; Davidson et al., 1977; Wlodek et al., 1980; Holland and Castleman, 1982; Froyd and Lovejoy, 2003), the stepwise ΔG values for clusters decreases exponentially as the cluster sizes increase and approaches to the bulk values when clusters containing more than ~ 8-10 molecules (Yu, 2005). Cluster compositions measured with an atmospheric pressure interface time-of-flight (APi-TOF) mass spectrometer during CLOUD experiments also show that the difference in the composition of positively and negatively charged clusters quickly decreases as the number of H_2SO_4 molecules increases from 1 to ~ 10 and exhibits little further changes (Schobesberger et al., 2015).

In the present TIMN model, we assume that both neutral and charged clusters have the same composition when s≥10 and the following extrapolation scheme is used to calculate $\Delta G_{s-1,s}$ for clusters up to s=10:

$$\Delta G_{s-1,s} = \Delta G_{s_1-1,s_1} + \frac{\left(\Delta G_{s_2-1,s_2} - \Delta G_{s_1-1,s_1}\right)\left(e^{-sc} - e^{-s_1 c}\right)}{\left(e^{-s_2 c} - e^{-s_1 c}\right)} \quad (10)$$

where $\Delta G_{s_1-1,s_1}$ is the stepwise mean Gibbs free energy change for H_2SO_4 addition for a specific type (neutral, positive, or negative) of clusters at s=s_1 that can be derived from QC calculation

and/or experimental measurements, and $\Delta G_{s_2-1,s_2}$ is the corresponding value for clusters at s=s_2 (=10 in the present study) that is calculated in the capillarity approximation accounting for the Kelvin effect. c in Eq. 10 is the exponential coefficient that determines how fast $\Delta G_{s-1,s}$ approaches to bulk values as s increases. In the present study, c is estimated from $\Delta G_{s-1,s}$ at s=2 and s=3 for neutral binary and ternary clusters for which experimental (Hanson and Lovejoy, 2006; Kazil et al., 2007) or quantum-chemical data (Table A3) are available. Apparently the interpolation approximation Eq. (10) is subject to uncertainty. Nevertheless, it is a reasonable approach to connect thermochemical properties of QC data for small binary and ternary clusters that cannot be adequately described by the capillarity approximation with those for large clusters that can be adequately described the very same capillarity approximation, and is the best approach we can come up with at this point in order to develop a model that can be applied to all conditions. Further QC and experimental studies of the thermodynamics of relatively larger clusters can help to reduce the uncertainty.

For clusters with $s \geq s_2$, the capillarity approximation is used to calculate $\Delta G_{s-1,s}$ as

$$\Delta G_{s-1,s} = -RT \ln(P/P_s) + \frac{2\sigma v_1 N_A}{r_s} \quad (11)$$

where P is the H_2SO_4 vapor pressure and P_s is the H_2SO_4 saturation vapor pressure over a flat surface with the same composition as the cluster. σ is the surface tension and v_1 is the volume of one H_2SO_4 molecule. r_s is the radius of the cluster and N_A is the Avogadro's number.

The scheme to calculate bulk $\Delta G_{s-1,s}$ ($s \geq 10$) for H_2SO_4-H_2O binary clusters has been described in Yu (2007). For ternary nucleation, both experiments (Schobesberger et al., 2015) and QC calculations (Table A4) indicate that the growth of relatively large clusters follows the s=a line (i.e, in the composition of ammonia bisulfate). In the present TIMN model, the bulk $\Delta G_{s-1,s}$ values for ternary clusters are calculated based on parameterized H_2SO_4 saturation vapor pressure over ammonia bisulfate as a function of temperature, derived by Martin et al. (1997) from vapor pressures measured at temperature between 27 ºC and º60 C, and surface tension measured at 298 K from Hyvarinen et al. (2005). The uncertainty in saturation vapor pressures and surface tension used in the calculation of the bulk $\Delta G_{s-1,s}$ values is another source of uncertainty in the TIMN

405 model, although it is likely to be small compared to other uncertainties as the nucleation is
406 generally limited by the formation of small clusters.
407 Figure 4 presents stepwise ($\overline{\Delta G}_{s-1,s}$) and cumulative (total) $\overline{\Delta G}_s$ Gibbs free energy changes
408 associated with the formation of neutral, positively charged, and negatively charged binary and
409 ternary clusters containing s H_2SO_4 molecules under the conditions specified in the figure caption.
410 The clusters are assumed to be in equilibrium with water (Yu, 2007) and ammonia (Fig. 3). As
411 seen from Fig. 4, the presence of NH_3 reduces the mean $\overline{\Delta G}_{s-1,s}$ for larger clusters, which can be
412 treated as the bulk binary H_2SO_4-H_2O solution (Schobesberger et al., 2015), by ~ 3 kcal mol^{-1},
413 indicating a substantial reduction in the H_2SO_4 vapor pressure over ternary solutions (Marti et al.,
414 1997). The comparison also shows that the influence of NH_3 on $\overline{\Delta G}_{s-1,s}$ of small clusters ($s \leq \sim 4$)
415 is much lower than that on larger ones and bulk solutions. For example, at [NH_3]=0.3 ppb, the
416 differences in $\overline{\Delta G}_{s-1,s}$ between binary and ternary positive ions with s=1 and neutral clusters with
417 s=2 are only 0.45 kcal mol^{-1} and ~ 1 kcal mol^{-1}, respectively. In the case of negative ions, zero
418 and 0.27−0.45 kcal mol^{-1} differences at $s \leq 2$ and s=3-4, respectively, were observed. The reduced
419 effect of ammonia on smaller clusters is explained (Tables A2-A4) by ammonia's weaker bonding
420 to smaller clusters than to larger ones, which in turn yields lower average NH_3 to H_2SO_4 ratios
421 (Fig. 3). It should be noted that QC data for positively charged clusters are very limited and the
422 interpolation approximation is subject to large uncertainty. In order for the nucleation on positive
423 ions to occur, the first step is for H_2SO_4 to attach to a positive ion that does not contain H_2SO_4.
424 Unlike negative ions, the effect of charge on the bonding of H_2SO_4 with positive ions is much
425 weaker and thus the stepwise Gibbs free energy change for the addition of one H_2SO_4 molecule to
426 form a positively charged cluster is likely to be similar to that of neutral clusters, i.e., decreasing
427 with cluster size. Therefore, the QC data for positively charged clusters containing one H_2SO_4
428 molecule provides a critical constrain. The success of the model in predicting the [NH_3] needed
429 for nucleation on positive ions to occur (see Section 3) show the usefulness of the first step data
430 and approximation.
431 As seen from Fig. 4, bonding of H_2SO_4 to small negatively charged clusters (s<3) is much
432 stronger than that to neutrals and positive ions. As a result, at s<3 the formation of negatively
433 charged clusters is barrierless ($\overline{\Delta G}_{s-1,s}$ <0). These small clusters cannot be considered as nucleated
434 particles because $\overline{\Delta G}_{s-1,s}$ (Fig. 4a) first increases and then decreases with growing s, reaching the
435 maximum barrier values at s = ~ 3 - 6. $\overline{\Delta G}_{s-1,s}$ can become positive for larger clusters due to the

charge effect decreasing quickly as the clusters are growing. The negative $\overline{\Delta G}_{s-1,s}$ for small clusters is not able to cancel the positive $\overline{\Delta G}_{s-1,s}$ for larger clusters and thus, to show properly the overall nucleation barrier, $\overline{\Delta G}_{s-1,s}$ for small clusters are set to zero when they are negative in the cumulative Gibbs free energy calculation. The effect of NH_3 on negative ions becomes important at $s \geq \sim 4$, when bonding between the clusters and NH_3 becomes strong enough to contaminate a large fraction of binary clusters with ammonia (Fig. 3). In contrast, the impact of NH_3 on neutral dimers and positively charged monomers of H_2SO_4, as well as on $\overline{\Delta G}_{s-1,s}$ for both positively charged and neutral clusters, monotonically decreases for all s, including $s \leq 5$.

$\overline{\Delta G}_{s-1,s}$ for charged and neutral clusters converge into the bulk values at $s = \sim 10$, when impact of the chemical identity of the core ion on the cluster composition becomes diffuse (Schobesberger et al., 2015) and when the contribution of the electrostatic effect to $\overline{\Delta G}_{s-1,s}$ becomes less than ~ 0.5 kcal mol^{-1}. The comparison of cumulative (total) $\overline{\Delta G}_s$ (Fig. 4b) indicates the lowest nucleation barrier for the case of negative ions, followed by positive ions and neutrals. The barrierless formation of clusters with s ranging from 1 to 3 substantially reduces the nucleation barrier for negatively charged ions and facilitates their nucleation. The presence of 0.3 ppb of NH_3 lowers the nucleation barrier for negative, positive and neutral clusters from ~17, 24 and 38 kcal mol^{-1} to 2, 7 and 16 kcal mol^{-1}, respectively. A relatively low nucleation barrier for charged ternary clusters is explained by the simultaneous effect of ionization and NH_3 which also reduces the size of the critical cluster (s^*).

It is important to note that the size of the critical cluster, commonly used to "measure" the activity of nucleation agents in the classical nucleation theory (Coffman and Hegg, 1995; Korhonen et al., 1999; Vehkamäki et al., 2002; Napari et al., 2002; Hamill et al., 1982) is no longer a valid indicator, when charged molecular clusters and small nanoparticles are considered. As seen from Fig. 4, positively charged ternary critical clusters (s^*=3-4) are smaller than the corresponding negatively charged ones (s^*=4-5); however, the nucleation barrier for ternary positive clusters under the condition specified in the figure caption is more than three times higher than that for ternary negatives ones.

2.4.3 Size- and composition- dependent H_2SO_4 evaporation rates

As we mentioned earlier, H_2SO_4 is the key atmospheric nucleation precursor driving the formation and growth of clusters in the ternary H_2SO_4-H_2O-NH_3 system while ions, H_2O, and NH_3 act to stabilize the H_2SO_4 clusters. The clustering thermodynamic data derived from QC calculations and measurements (Section 2.3) are used to constrain size- and composition-dependent Gibbs free energy changes and evaporation rates of H_2SO_4 which are critically important. Average or effective rates of H_2SO_4 molecule evaporation from positively charged, negatively charged, and neutral clusters containing s H_2SO_4 molecules ($\bar{\gamma}_s^{+,-,0}$) are calculated from $\overline{\Delta G}_{s-1,s}$ as:

$$\bar{\gamma}_s^{+,-,0} = \beta_{s-1}^{+,-,0} N^{o} \exp\left(\frac{\overline{\Delta G}_{s-1,s}}{RT}\right) \quad (12)$$

where N^{o} is as defined in Eq. (7). The present model assumes only a single H_2SO_4 molecule evaporates, i.e. no water ligands, for instance, are attached to it. This is likely the dominant evaporation pathway as hydrated H_2SO_4 molecules are generally more stable.

Figure 5 gives the mean evaporation rate ($\bar{\gamma}$) of an H_2SO_4 molecule from these clusters under the conditions corresponding to Fig. 4. The shapes of $\bar{\gamma}$ curves are similar to those of $\overline{\Delta G}_{s-1,s}$ (Fig. 4a) as $\bar{\gamma}$ values are largely controlled by $\overline{\Delta G}_{s-1,s}$ (Eq. 12). The presence of ammonia, as expected, significantly reduces the vapor pressure of H_2SO_4 over bulk aerosol (Marti et al., 1997), and, hence, the H_2SO_4 evaporation rate. The evaporation rates of both neutral and positive clusters decrease as s increases, and the positive clusters are uniformly more stable than corresponding neutral clusters. $\bar{\gamma}$ for negative ions first increases and then decreases as s increases, peaking around s= ~3 - 6. The presence of NH_3 reduces the evaporation rates of larger clusters by more than two orders of magnitude and the effect decreases for smaller clusters, as the binding of NH_3 to small neutral and charged clusters are weaker compared to that for larger clusters (Fig. 4). [NH_3] influences the average NH_3:H_2SO_4 ratio (Fig. 3) and the evaporation rates of these small clusters. The nucleation rates, limited by formation of small clusters (s<~ 5), depend strongly on the stability or evaporation rate of these small clusters. While the binding of NH_3 to small neutral and charged clusters is weaker compared to that to larger clusters, small clusters containing NH_3 are much more stable than those without (Fig. 4) and thus ammonia is important for nucleation.

3. TIMN rates and comparisons with CLOUD measurements

The evolution of cluster/particle size distributions can be obtained by solving the dynamic equations 1-6. Since the concentrations of clusters of all sizes are predicted, the nucleation rates in

the kinetic model can be calculated for any cluster size larger than the critical size of neutral clusters ($i > i^*$) (Yu, 2006b),

$$J_i = J_i^+ + J_i^- + J_i^0 = \beta_{i,1}^+ N_1^0 N_i^+ - \gamma_i^+ N_{i+1}^+ + \beta_{i,1}^- N_1^0 N_i^- - \gamma_i^- N_{i+1}^- + \beta_{i,1}^0 N_1^0 N_i^0 - \gamma_i^0 N_{i+1}^0 \quad (13)$$

where J_i^+, J_i^-, and J_i^0 are nucleation rates associated with positive, negative, and neutral clusters containing i H_2SO_4 molecules. As a result of scavenging by pre-existing particles or wall loss, the steady state J_i decreases as i increases. To compare with CLOUD measurements, we calculate nucleation at cluster mobility diameter of 1.7 nm ($J_{1.7}$).

Many practical applications require information on the steady state nucleation rates. For each nucleation case presented in this paper, constant values of $[H_2SO_4]$ (i.e., N_1^0), $[NH_3]$, T, RH, Q, and $L_i^{+,-,0}$ are assumed. The pre-existing particles with fixed surface area or wall loss serve as a sink for all clusters. Under a given condition, cluster distribution and nucleation rate reach steady state after a certain amount of time. We calculate size-dependent coefficients for a given case, and then solve equations (1-6) to obtain the steady state cluster distribution and nucleation rate, with the approach described in Yu (2006b).

Figure 6 shows a comparison of the model TIMN rates $J_{1.7}$ with CLOUD measurements, as a function of $[NH_3]$ under two ionization rates. It should be noted that Dunne et al. (2016) developed a simple empirical parameterization (denoted thereafter as "CLOUDpara") of binary, ternary and ion-induced nucleation rates in CLOUD measurements as a function of $[NH_3]$, $[H_2SO_4]$, T, and negative ion concentration. The predictions of CLOUDpara (Dunne et al., 2016) and ACDC based on nucleation thermochemistry obtained using RI-CC2//B3LYP method (McGrath et al., 2012; Kurten et al., 2016) are also presented in Fig. 6 for comparisons.

Like the CLOUD measurements, the TIMN predictions reveal a complex dependence of $J_{1.7}$ on $[NH_3]$, and an analysis of the TIMN results shows this behavior can be explained by the differing responses of negative, positive and neutral clusters to the presence of ammonia (Fig. 4). Under the conditions specified in Fig. 6, nucleation is dominated by negative ions for $[NH_3]$ <~0.5 ppb, by both negative and positive ions for $[NH_3]$ from ~0.5 ppb to ~10 ppb (with background ionization), or ~20 ppb (with pion-enhanced ionization), and by neutrals at higher $[NH_3]$. According to TIMN, $[NH_3]$ of at least 0.6–1 ppb are needed before positive ions contribute significantly to nucleation rates – in good agreement with the threshold found in the CLOUD experiments (Kirkby et al., 2011; Schobesberger et al., 2015). TIMN simulations also extend CLOUD data at $[NH_3]$ of ~1 ppb to include a "zero-sensitivity zone" in the region of 1-10 ppb, followed by a region of strong sensitivity of $J_{1.7}$ to $[NH_3]$ commencing at $[NH_3]$ > ~10-20 ppb. The

latter zone may have important implications for NPF in heavily polluted regions, including much of India and China, where [NH_3] may exceed 10-20 ppb (Behera and Sharma, 2010; Meng et al., 2017). It is noteworthy in Fig. 6 that the dependence of $J_{1.7}$ on [NH_3] and Q predicted by the ACDC model (McGrath et al., 2012) and the CLOUD data parameterization (Dunne et al., 2016) deviate substantially from the experimental data as well as the TIMN simulations. The CLOUDpara does not consider impacts of positive ions and such key controlling parameters as RH and surface area of pre-existing particles. Dunne et al. (2016) reported that CLOUDpara is also very sensitive to the approach to parameterize T dependence, showing that the contribution of ternary ion-induced nucleation to NPF below 15 km altitude has grown from 9.6% to 37.5%, after the initial empirical temperature function was replaced with a simpler one.

Figure 7 presents a more detailed comparison of TIMN simulations with CLOUD measurements of $J_{1.7}$ as a function of [H_2SO_4], T, and RH. The TIMN model reproduces both the absolute values of $J_{1.7}$ and its dependencies on [H_2SO_4], T, and RH, in a wide range of temperatures (T=208 – 292 K) and [H_2SO_4] (5×10^5 – 5×10^8 cm^{-3}). As expected, nucleation rates are very sensitive to [H_2SO_4] and T. For example, $J_{1.7}$ increases by three to five orders of magnitude with an increase in [H_2SO_4] of a factor of 10, and by roughly one order of magnitude for a temperature decrease of 10 degree, except in cases where the nucleation rate is limited by Q (for example, [H_2SO_4] =~10^8 – 10^9 cm^{-3} at T=278 K and 292 K, shown in Fig. 7a). The key difference between CLOUDpara and TIMN predictions is that $d\ln J_{1.7}/d\ln[H_2SO_4]$ ratio predicted by CLOUDpara is nearly constant while TIMN shows that this ratio depends on both [H_2SO_4] and T. The CLOUD measurements taken at T=278 K clearly show (in agreement with the TIMN) that $d\ln J_{1.7}/d\ln[H_2SO_4]$ is not constant. CLOUDpara overestimates $J_{1.7}$ compared to both measurements and TIMN simulations, except for the case, when T=278 K and [H_2SO_4] ranges from ~7×10^6 to 5×10^7 cm^{-3}, with deviation of CLOUDpara from experimental data and TIMN growing with the lower temperature.

Both CLOUD measurements and TIMN simulations (Fig. 7b) show an important influence of RH on nucleation rates (which is neglected in both the CLOUDpara and ACDC models). In particular, CLOUD measurements indicate 1-5 order of magnitude rise in $J_{1.7}$ after RH increases from 10% to 70-80% and a stronger effect of RH on nucleation rates at higher temperatures under the conditions shown in Fig. 7b. The RH dependence of $J_{1.7}$ predicted by the TIMN model is consistent with measurements, being slightly weaker than the measured at high RH.

Figure 8 compares TIMN model predictions with all 377 data points of CLOUD measurements reported in data Table S1 of Dunne et al. (2016). The vertical error bars show the range of J_{model} associated with the uncertainty in the [H_2SO_4] measured (-50%, +100%). The effect of uncertainty in measured [NH_3] (-50%, +100%) is not included. At the presence of ionization (Fig. 8a), J_{model} agrees with CLOUD measurements within the uncertainties under mainly all conditions, although

564 J_{model} tends to be slightly lower than J_{obs} when T=292 – 300 K and J_{obs} is relatively small (<~ 1 cm^{-3}s^{-1}). For the neutral nucleation (Fig. 8b), the model agrees well with observations at low T (T=205 – 223 K) but deviates from observations as T increases. The under-prediction of the model for neutral nucleation at T=278 – 300 K cannot be explained by the uncertainties in measured [H_2SO_4] and [NH_3]. Apparently for neutral nucleation the model predicts much stronger temperature dependence than the CLOUD measurements. The possible reasons for the difference include the uncertainties in both the model (especially the thermodynamics data and approximation) and measurements. The contamination (by amines) in the CLOUD measurements (Kirkby et al., 2011) can be another possible reason. The level of contamination in the cloud chamber appears to increase with temperature (Kurten et al., 2016), which may explain the good agreement at low T and increased deviation at higher T. Further research is needed to identify the source of the difference for neutral ternary nucleation at high T.

4. Summary

A comprehensive kinetically-based H_2SO_4-H_2O-NH_3 ternary ion-mediated nucleation (TIMN) model, constrained with thermodynamic data from quantum-chemical calculations and laboratory measurements, has been developed and used to shed a new light on physico-chemical processes underlying the effect of ammonia on NPF. We show that the stabilizing effect of NH_3 grows with the cluster size, and that the reduced effect of ammonia on smaller clusters is caused by weaker bonding that in turn yields lower average NH_3 to H_2SO_4 ratios. NH_3 was found to impact nucleation barriers for neutral, positively charged, and negatively charged clusters differently due to the large difference in the binding energies of NH_3, H_2O, and H_2SO_4 to small clusters of different charging states. The lowest and highest nucleation barriers are observed in the case of negative ions and neutrals, respectively. Therefore, nucleation of negative ions is favorable, followed by nucleation of positive ions and neutrals. Different responses of negative, positive and neutral clusters to ammonia result in a complex dependence of ternary nucleation rates on [NH_3]. The TIMN model reproduces both the absolute values of nucleation rates and their dependencies on the key controlling parameters and agrees with the CLOUD measurements for all the cases at the presence of ionization. For the neutral ternary nucleation, the model agrees well with observations at low temperature but deviates from observations as temperature increases.

The TIMN model developed in the present study may subject to uncertainties associated with the uncertainties in thermodynamic data and interpolation approximation for pre-nucleation clusters. Further measurements and quantum calculations, especially for relatively larger clusters, are needed to reduce the uncertainties. While the TIMN model predicts nucleation rates in a good overall agreement with the CLOUD measurements, its ability to explain the NPF events observed in the real atmosphere is yet to be quantified and will be investigated in further studies.

Appendix

A1. Quantum-chemical studies of neutral and charged binary and ternary clusters

Thermochemical data for small neutral and charged binary H_2SO_4-H_2O and ternary H_2SO_4-H_2O-NH_3 clusters has been reported in a number of earlier publications (Bandy and Ianni, 1998; Ianni and Bandy, 1999; Torpo et al., 2007; Nadykto et al., 2008; Herb et al., 2011, 2013; Temelso et al., 2012a, b; DePalma et al., 2012; Ortega et al., 2012; Chon et al., 2014; Husar et al., 2014; Henschel et al., 2014, 2016; Kurten et al., 2015). The PW91PW91/6-311++G(3df,3pd) method, which is a combination of the Perdue-Wang PW91PW91 density functional with the largest Pople 6-311++G(3df,3pd) basis set, has thoroughly been validated and agrees well with existing experimental data. In earlier studies, this method has been applied to a large variety of atmospherically-relevant clusters (Nadykto et al. 2006, 2007a, b, 2008, 2014, 2015; Torpo et al. 2007; Zhang et al., 2009; Elm et al. 2012; Leverentz et al. 2013; Xu and Zhang, 2012; Xu and Zhang, 2013; Elm et al., 2013; Zhu et al. 2014; Bork et al. 2014; Elm and Mikkelsen, 2014; Peng et al. 2015; Miao et al 2015; Chen et al., 2015; Ma et al., 2016) and has been shown to be well suited to study the H_2SO_4-H_2O and H_2SO_4-H_2O-NH_3 clusters, as evidenced by a very good agreement of the computed values with measured cluster geometries, vibrational fundamentals, dipole properties and formation Gibbs free energies (Nadykto et al., 2007a, b, 2008, 2014, 2015; Herb et al., 2013; Elm et al., 2012, 2013; Leverentz et al., 2013; Bork et al., 2014) and with high level ab initio results (Temelso et al., 2012a, b; Husar et al., 2012; Bustos et al., 2014).

We have extended the earlier QC studies of binary and ternary clusters to larger sizes. The computations have been carried out using Gaussian 09 suite of programs (Frish et al., 2009). In order to ensure the quality of the conformational search we have carried out a thorough sampling of conformers. We have used both basin hopping algorithm, as implemented in Biovia Materials Studio 8.0, and locally developed sampling code. The sampling code is based on the following principle: mesh, with molecule to be added to the cluster placed in the mesh nodes, is created around the cluster, and blind search algorithm is used to generate the guess geometries. The mesh density and orientation of molecules are variable, as well as the minimum distance between molecules and cluster. Typically, for each cluster of a given chemical composition a thousand to several thousands of isomers have been sampled. We used a three-step optimization procedure, which includes (i) pre-optimization of initial/guess geometries by semi-empirical PM6 method, separation of the most stable isomers located within 15 kcal mol^{-1} of the intermediate global minimum and duplicate removal, followed by (ii) optimization of the selected isomers meeting the aforementioned stability criterion by PW91PW91/CBSB7 method and (iii) the final optimization of the most stable at PW91PW91/CBSB7 level isomers within 5 kcal mol^{-1} of the current global minimum using PW91PW91/6-311++G(3df,3pd) method. Typically, only ~4-30% of initially

sampled isomers reach the second (PW91PW91/CBSB7) level, where ~10-40% of isomers optimized with PW91PW91/CBSB7 are selected for the final run. Typically, the number of equilibrium isomers of hydrated clusters is larger than that of unhydrated ones of similar chemical composition. Table A1 shows the numbers of isomers converged at the final PW91PW91/6-311++G(3df,3pd) optimization step for selected clusters and HSG values of the most stable isomers used in the present study. The number of isomers optimized at the PW91PW91/6-311++G(3df,3pd) level of theory varies from case to case, typically being in the range of ~10-200.

The computed stepwise enthalpy, entropy, and Gibbs free energies of cluster formation have been thoroughly evaluated and used to calculate the evaporation rates of H_2SO_4 from neutral, positive and negative charged clusters.

A1.1 Positively charged clusters

Table A2 presents the computed stepwise Gibbs free energy changes under standard conditions (ΔG^o) for positive binary and ternary clusters, along with the corresponding experimental data or semi-experimental estimates. Figure 2 in the main text shows ΔG associated with the addition of water (ΔG^o_{+W}), ammonia (ΔG^o_{+A}), and sulfuric acid (ΔG^o_{+S}) to binary and ternary clusters as a function of the cluster hydration number *w*. Both the absolute values and trends in ΔG^o_{+W} derived from calculations are in agreement with the laboratory measurements within the uncertainty range of ~1-2 kcal mol^{-1} for both QC calculations and measurements. This confirms the efficiency and precision of QC methods in calculating thermodynamic data needed for the development of nucleation models. Nevertheless, it should be noted that the uncertainties in computed free energies of 1-2 kcal mol^{-1} may lead to large uncertainty in predicted particle formation rates. By increasing or decreasing all Gibbs free energies by 1 kcal mol^{-1}, Kürten at al. (2016) showed that, depending on the conditions, the modeled particle formation rate can change from less than an order of magnitude to several orders of magnitude. Uncertainties estimated by Kürten at al. (2016) represent the upper limit because computed free energies may be overestimated for some clusters and underpredicted for others that leads to partial or, in some case, full error cancelation.

A1.2 Neutral clusters

Table A3 presents the computed stepwise Gibbs free energy changes for the formation of ternary $S_sA_aW_w$ clusters under standard conditions. The corresponding binary electrically neutral clusters can be found in previous publications (e.g., Nadykto et al., 2008; Herb et al., 2011). The thermodynamic properties of the S_1A_1 have been reported in a number of computational studies (e.g., Herb et al., 2011; Kurten et al., 2007; Nadykto and Yu, 2007). However, most of these studies, except for Nadykto and Yu (2007) and Henschel et al. (2014; 2016), did not consider the impact of H_2O on cluster thermodynamics. We have extended the earlier studies of Nadykto and

Yu (2007) and Herb et al. (2011) to larger clusters up to S_4A_5 (no hydration) and up to S_2A_2 (hydration included). The free energy of binding of NH_3 to H_2SO_4 (or H_2SO_4 to NH_3) obtained using our method is -7.77 kcal mol^{-1} that is slightly more negative than values reported by other groups (-6.6 −-7.61 kcal mol^{-1}) and within less than 0.5 kcal mol^{-1} of the experimental value of -8.2 kcal mol^{-1} derived from CLOUD measurements (Kurten et al., 2015).

As it may be seen from Table A3, the NH_3 binding to $S_{1\text{-}2}W_w$ weakens as *w* increases. The average ΔG^o_{+W} for S_1W_w formation derived from a combination of laboratory measurements and quantum chemical studies are -3.02, -2.37, and -1.40 kcal mol^{-1} for the first, second, and third hydration, respectively (Yu, 2007). This indicates that a large fraction of H_2SO_4 monomers in the Earth's atmosphere is likely hydrated. Therefore, the decreasing NH_3 binding strength to hydrated H_2SO_4 monomers implies that RH (and T) will affect the relative abundance of H_2SO_4 monomers containing NH_3. Currently, no experimental data or observations are available to evaluate the impact of hydration (or RH) on ΔG^o_{+A}. Table A3 shows that the presence of NH_3 in H_2SO_4 clusters suppress hydration and that ΔG^o_{+W} for S_2A_2 falls below -2.0 kcal mol^{-1}. This is consistent with earlier studies by our group (Herb et al., 2011) and others (Henschel et al., 2014, 2016) showing that large S_nA_n clusters (*n>2*) are not hydrated under typical atmospheric conditions. In the present study, the hydration of neutral S_nA_n clusters at *n>2* is neglected, due to the lack of thermodynamic data.

The number of NH_3 molecules in the cluster (or H_2SO_4 to NH_3 ratio) significantly affects ΔG^o_{+S} and ΔG^o_{+A} values. For example, ΔG^o_{+S} for S_3A_a clusters increases from -7.08 kcal mol^{-1} to -16.92 kcal mol^{-1} and ΔG^o_{+A} decreases from -16.14 kcal mol^{-1} to -8.93 kcal mol^{-1} as *a* is growing from 1 to 3. For S_4A_a clusters, ΔG^o_{+S} is increasing from -7.48 kcal mol^{-1} to -16.26 kcal mol^{-1} and ΔG^o_{+A} decreases from -17.16 kcal mol^{-1} to -11.34 kcal mol^{-1} as *a* increases from 2 to 4. ΔG^o_{+A} for S_4A_1 cluster is by 1.38 kcal mol^{-1} less negative than that for S_4A_2. ΔG^o_{+S} for the S_4A_1 cluster is also quite low (-4.16 kcal mol^{-1}) that might indicate the possible existence of a more stable S_4A_1 isomer, which is yet to be identified. In the presence of NH_3, the uncertainty in the thermochemistry data for S_4A_1 will not significantly affect ternary nucleation rates because most of S_4-clusters contain 3 or 4 NH_3 molecules.

For the S_sA_a clusters with *s=a*, ΔG^o_{+A} increases as cluster is growing while ΔG^o_{+S} first increases significantly as S_1A_1 is converting into S_2A_2 and then levels off as S_2A_2 is converting into S_4A_4. We also observe a significant drop in ΔG^o_{+A} in the case when NH_3/H_2SO_4 ratio exceeds 1. This finding is consistent with the ACDC model calculation showing that growth of neutral S_sA_a clusters follows the *s=a* pathway (Schobesberger et al., 2015).

A1.3 Negative ionic clusters

Table A4 shows ΔG_{+W}, ΔG_{+A}, and ΔG_{+S} needed to form negatively charged clusters under standard conditions, along with available semi-experimental values (Froyd and Lovejoy, 2003). H_2O binding to negatively charged S^-S_s clusters significantly strengths with increasing *s*, from ΔG^o_{+W} = -0.61 −-1.83 kcal mol^{-1} at *s*=1-2 to ΔG^o_{+W} = -3.5 kcal mol^{-1} at *w*=1 and -2.25 kcal mol^{-1} at *w*=4 at *s*=4. ΔG^o_{+W} values at *s*=3 and 4 are slightly more negative (by ~ 0.1 – 0.9 kcal mol^{-1}) than those reported by Froyd and Lovejoy (2003). Just like H_2O binding, NH_3 binding to S^-S_s at *s*<3 is very weak, with ΔG^o_{+A} ranging from +2.81 kcal mol^{-1} at *s*=0 to -4.85 kcal mol^{-1} at *s*=2. However, it significantly increases as *s* is growing. In particular, at *s*≥3 ΔG^o_{+A} is ranging from -11.89 kcal mol^{-1} for $S^-S_3A_1$ to -15.37 kcal mol^{-1} for $S^-S_4A_1$. NH_3 clearly cannot get into small negative ions. However, it can easily attach to larger negative ions with *s*≥3 that is consistent with CLOUD measurements (Schobesberger et al., 2015). Since hydration weakens NH_3 binding in $S^-S_3A_1W_w$ and $S^-S_4A_1W_w$ clusters, its impacts on the cluster formation and nucleation rates may potentially be important.

In contrast to H_2O and NH_3, binding of H_2SO_4 to small negative ions (*s*<3) is very strong. These ions are very stable even when they contain no NH_3 or H_2O molecules. High electron affinity of H_2SO_4 molecules results in the high stability of S^-S_s at *s*=1-2. However, the charge effect reduces as *s* is growing. In particular, ΔG^o_{+S} of S^-S_s drops from -32.74 kcal mol^{-1} at *s*=1 to -10.58 kcal mol^{-1} and -8.28 kcal mol^{-1} at *s*=3 and 4, respectively. At the same time, ΔG^o_{+A} increases from 0.08 kcal mol^{-1} (*s*=1) to -11.89 kcal mol^{-1} (*s*=3) and -15.37 kcal mol^{-1} (*s*=4). The hydration of S^-S_s at *s*=3, 4 enhances the strength of H_2SO_4 binding, especially at *s=4*. ΔG^o_{+S} values for $S^-S_{3-4}W_w$ are consistently ~1.5 – 3 kcal mol^{-1} less negative than the corresponding semi-experimental estimates (Table A4). The possible reasons behind the observed systematic difference are yet to be identified and include the use of low-level *ab initio* HF method to compute reaction enthalpies and uncertainties in experimental enthalpies in studies by Froyd and Lovejoy (2003).

NH_3 binding to S^-S_3 significantly enhances the stability of H_2SO_4 in the cluster by ~7 kcal mol^{-1} compared to ΔG^o_{+S} for the corresponding binary counterpart. The binding of the second NH_3 to S^-S_3A to form $S^-S_3A_2$ is much weaker (ΔG^o_{+A}= -7.27 kcal mol^{-1}) that that of the first NH_3 molecule (ΔG^o_{+A}= -11.89 kcal mol^{-1}). This indicates that most of $S^-S_3A_a$ can only contain one NH_3 molecule, in a perfect agreement with the laboratory study of Schobesberger et al. (2015). In the case of S^-S_4, binding of the first (ΔG^o_{+A}= -15.37 kcal mol^{-1}) and second (and -12.23 kcal mol^{-1}) NH_3 molecules to the cluster is quite strong, while the attachment of NH_3 leads to substantial stabilization of H_2SO_4 in the cluster, as evidenced by ΔG^o_{+S} growing from -8.28 kcal mol^{-1}at *a=0* to -11.76 kcal mol^{-1}and -16.71 kcal mol^{-1} at *a=1* and *a=2*, respectively. The NH_3 binding free energy to $S^-S_4A_2$ (to form $S^-S_4A_3$) drops to -7.59 kcal mol$^{-1,}$ indicating, in agreement with the CLOUD measurements (Schobesberger et al., 2015) that most of S^-S_4 clusters contain 1 or 2 NH_3 molecules.

Acknowledgments. The authors thank Richard Turco (Distinguished Professor Emeritus, UCLA) for comments that helped to improve the manuscript. This study was supported by NSF under grant 1550816, NASA under grant NNX13AK20G, and NYSERDA under contract 100416. ABN would like to thank the Russian Science Foundation and the Ministry of Science and Education of Russia (under grants 1.6198.2017/6.7 and 1.7706.2017/8.9) for support and the Center of Collective Use of MSTU Stankin for providing resources.

Data availability. All relevant data are available in the article, or from the corresponding authors upon request.

References

Almeida, J., et al., Molecular understanding of sulphuric acid–amine particle nucleation in the atmosphere, Nature, 502, 359-363, 2013.

Ball, S. M., Hanson, D. R., Eisele, F. L., and McMurry, P. H., Laboratory studies of particle nucleation: Initial results for H_2SO_4, H_2O, and NH_3 vapors, J. Geophys. Res., 104, 23709-23718, 10.1029/1999JD900411, 1999.

Bandy, A.R. and Ianni, J.C., Study of the hydrates of H_2SO_4 using density functional theory. The Journal of Physical Chemistry A, 102(32), pp.6533-6539, 1998.

Behera, S. N.,and M. Sharma, Investigating the potential role of ammonia in ion chemistry of fine particulate matter formation for an urban environment, The Science of the Total Environment, 408(17), 3569-3575, 2010.

Benson, D. R.,M. E. Erupe, and S.-H. Lee, Laboratory-measured H_2SO_4-H_2O-NH_3 ternary homogeneous nucleation rates: Initial observations, Geophys. Res. Lett., 36, L15818, doi:10.1029/2009GL038728, 2009.

Bork, N., Du, L., Reiman, H., Kurtén, T. and Kjaergaard, H.G., Benchmarking ab initio binding energies of hydrogen-bonded molecular clusters based on FTIR spectroscopy, Journal of Physical Chemistry A, 118(28), 5316-5322, 2014.

Bustos, D.J., Temelso, B. and Shields, G.C., Hydration of the Sulfuric Acid–Methylamine Complex and Implications for Aerosol Formation. The Journal of Physical Chemistry A, 118(35), pp.7430-7441, 2014.

Butler, T., Vermeylen, F., Lehmann, C. M., Likens, G. E., & Puchalski, M.. Increasing ammonia concentration trends in large regions of the USA derived from the NADP/AMoN network. Atmospheric Environment, 146, 132–140. 2016.

777 Chen, M., M. Titcombe, J. Jiang, C. Kuang, M. L. Fischer, E. Edgerton, F. L. Eisele, J. I. Siepmann,
778 D. H. Hanson, J. Zhao, and P. H. McMurry, Acid-base chemical reaction model for nucleation
779 rates in the polluted boundary layer. Proc. Nat. Acad. Sci., 109, 18713–18718, 2012.
780 Chon, N.L., Lee, S.H. and Lin, H., A theoretical study of temperature dependence of cluster
781 formation from sulfuric acid and ammonia. Chemical Physics, 433, pp.60-66, 2014.
782 Coffman, D. J., and Hegg, D. A., A preliminary study of the effect of ammonia on particle
783 nucleation in the marine boundary layer, J. Geophys. Res., 100, 7147-7160, 1995.
784 Davidson, J. A., Fehsenfeld, F.C., Howard, C.J.: The heats of formation of NO_3^- and NO_3^-
785 association complexes with HNO_3 and HBr, Int. J. Chem. Kinet., 9, 17, 1977.
786 Dawson M.L., et al., Simplified mechanism for new particle formation from methanesulfonic acid,
787 amines and water via experiments and ab initio calculations, Proc Natl Acad Sci USA
788 109:18719–18724, 2012.
789 DePalma, J.W., Bzdek, B.R., Doren, D.J. and Johnston, M.V., Structure and energetics of
790 nanometer size clusters of sulfuric acid with ammonia and dimethylamine, Journal of Physical
791 Chemistry A, 116(3), pp.1030-1040, 2012.
792 Doyle, G. J., Self-nucleation in the sulfuric acid-water system, J. Chem. Phys.,35, 795–799, 1961.
793 Dunne, E. M., et al., Global particle formation from CERN CLOUD measurements, Science,
794 doi:10.1126/science.aaf2649, 2016.
795 Duplissy J., et al., Effect of ions on sulfuric acid-water binary particle formation: 2. Experimental
796 data and comparison with QC-normalized classical nucleation theory, J. Geophys. Res. Atmos.,
797 121, 1752–1775, doi:10.1002/2015JD023539, 2016.
798 Elm, J. and Mikkelsen, K.V., Computational approaches for efficiently modelling of small
799 atmospheric clusters, Chemical Physics Letters, 615, 26-29, 2014.
800 Elm, J., Bilde, M. and Mikkelsen, K.V., Assessment of binding energies of atmospherically
801 relevant clusters, Physical Chemistry Chemical Physics, 15(39), 16442-16445, 2013.
802 Elm, J., Bilde, M. and Mikkelsen, K.V., Assessment of density functional theory in predicting
803 structures and free energies of reaction of atmospheric prenucleation clusters, Journal of
804 chemical theory and computation, 8(6), 2071-2077, 2012.
805 Frisch, M. J., Trucks, G. W., Schlegel, H. B., Scuseria, G. E., Robb, M. A., Cheeseman, J. R.,
806 Scalmani, G., Barone, V., Mennucci, B., et al., Gaussian 09, Gaussian, Inc., Wallingford CT,
807 2009.
808 Froyd K. D., and Lovejoy E. R., Bond energies and structures of ammonia-sulfuric acid positive
809 cluster ions, J. Phys. Chem. A, 116(24), 5886–5899, doi:10.1021/jp209908f, 2012.
810 Froyd, K. D., and Lovejoy, E. R., Experimental thermodynamics of cluster ions composed of
811 H_2SO_4 and H_2O. 1. Positive ions, J. Phys. Chem. A, 107, 9800–9811, 2003.

812 Froyd, K. D., and Lovejoy, E. R., Experimental thermodynamics of cluster ions composed of
813 H_2SO_4 and H_2O. 2. Measurements and ab initio structures of negative ions, J. Phys. Chem. A,
814 107, 9812–9824, 2003.
815 Froyd, K. D., and Lovejoy, E. R., Experimental thermodynamics of cluster ions composed of
816 H2SO4 and H2O. 1. Positive ions, J. Phys. Chem. A, 107, 9800–9811, 2003.
817 Froyd, K. D., Ion induced nucleation in the atmosphere: Studies of NH_3, H_2SO_4, and H_2O cluster
818 ions, Ph.D. thesis, Univ. of Colo., Boulder, 2002.
819 Glasoe, W. A., Volz, K., Panta, B., Freshour, N., Bachman, R., Hanson, D. R., McMurry, P. H.,
820 and Jen, C.. Sulfuric acid nucleation: An experimental study of the effect of seven bases. Journal
821 of Geophysical Research: Atmospheres, 120(5), 1933-1950, 2015.
822 Hamill, P., Turco, R. P., Kiang, C. S., Toon, O. B., & Whitten, R. C., An analysis of various
823 nucleation mechanisms for sulfate particles in the stratosphere. Journal of Aerosol Science, 13,
824 561–585, 1982.
825 Hanson, D. R., and F. Eisele, Diffusion of H_2SO_4 in humidified nitrogen: Hydrated H_2SO_4, J. Phys.
826 Chem. A, 104, 1715 – 1719, 2000.
827 Hanson, D. R., and F. L. Eisele, Measurement of prenucleation molecular clusters in the NH_3,
828 H_2SO_4, H_2O system, J. Geophys. Res., 107(D12), 4158, doi:10.1029/2001JD001100, 2002.
829 Hanson, DR., Lovejoy, ER, Measurement of the thermodynamics of the hydrated dimer and
830 trimers, J. Phys. Chem. A 110: 9525-9538 DOI: 10.1021/jp062844w, 2006.
831 Henschel, H., J. C. A. Navarro, T. Yli-Juuti, O. Kupiainen-Määttä, T. Olenius, I. K. Ortega, S. L.
832 Clegg, T. Kurtén, I. Riipinen, and H. Vehkamäki, Hydration of atmospherically relevant
833 molecular clusters: Computational chemistry and classical thermodynamics, J. Phys. Chem. A,
834 118, 2599–2611, 2014.
835 Henschel, H., T. Kurtén, and H. Vehkamäki, Computational study on the effect of hydration on
836 new particle formation in the sulfuric acid/ammonia and sulfuric acid/dimethylamine systems,
837 J. Phys. Chem. A, 120, 1886–1896, doi:10.1021/acs.jpca.5b11366, 2016.
838 Herb, J., Y. Xu, F. Yu, and A. B. Nadykto, Large Hydrogen-Bonded Pre-Nucleation $(HSO_4^-)(H_2SO_4)_m(H_2O)_k$ and $(HSO_4^-)(NH_3)(H_2SO_4)_m(H_2O)_k$ Clusters in the Earth's Atmosphere, J.
840 Phys. Chem., A, 117, 133-152, DOI: 10.1021/jp3088435, 2013.
841 Herb., J., A. Nadykto, and F. Yu, Large Ternary Hydrogen-Bonded Pre-Nucleation Clusters in the
842 Earth's Atmosphere, Chemical Physics Letters, 518, 7-14, 10.1016/j.cplett.2011.10.035, 2011.
843 Holland, P. M., and Castleman, A. W., Jr.: Thomson equation revisited in light of ion-clustering
844 experiments, J. Phys. Chem.; 86, 4181-4188, 1982.
845 Hoppel, W.A., and G. M. Frick, Ion-aerosol attachment coefficients and the steady-state charge
846 distribution on aerosols in a bipolar ion environment, Aerosol Sci. Tech., 1-21, 1986.

847 Husar, D.E., Temelso, B., Ashworth, A.L. and Shields, G.C., Hydration of the bisulfate ion:
848 atmospheric implications. The Journal of Physical Chemistry A, 116(21), pp.5151-5163, 2012.
849 Hyvärinen, A., T. Raatikainen, A. Laaksonen, Y. Viisanen, and H. Lihavainen, Surface tensions
850 and densities of H_2SO_4 + NH_3 + water solutions, Geophy. Res. Lett., 32, L16806,
851 doi:10.1029/2005GL023268, 2005.
852 Ianni, J.C. and Bandy, A.R., A Density Functional Theory Study of the Hydrates of NH_3-H_2SO_4
853 and Its Implications for the Formation of New Atmospheric Particles. The Journal of Physical
854 Chemistry A, 103(15), pp.2801-2811, 1999.
855 Jacobson, M., Turco, R., Jensen, E. and Toon O.: Modeling coagulation among particles of
856 different composition and size, Atmos. Environ., 28, 1327-1338, 1994.
857 Jolly, William L., Modern Inorganic Chemistry (2nd Edn.). New York: McGraw-Hill. ISBN 0-07-
858 112651-1, 1991.
859 Kazil, J., Lovejoy, E. R., Jensen, E. J., and Hanson, D. R.: Is aerosol formation in cirrus clouds
860 possible?, Atmos. Chem. Phys., 7, 1407-1413, https://doi.org/10.5194/acp-7-1407-2007, 2007.
861 Kebarle, P., S. K. Searles, A. Zolla, J. Scarborough, and M. Arshadi, J. Am. Chem. Soc., 89, 6393,
862 1967.
863 Kim, T. O., T. Ishida, M. Adachi, K. Okuyama, and J. H. Seinfeld, Nanometer-Sized Particle
864 Formation from NH_3/SO_2/H_2O/Air Mixtures by Ionizing Irradiation, Aerosol Science and
865 Technology, 29, 112-125, 1998.
866 Kirkby, J., Curtius, J., Almeida, J., Dunne, E., Duplissy, J., et al., The role of sulfuric acid,
867 ammonia and galactic cosmic rays in atmospheric aerosol nucleation, Nature, 476, 429–433,
868 2011.
869 Korhonen, P., Kulmala, M., Laaksonen, A., Viisanen, Y., McGraw, R., and Seinfeld, J. H., Ternary
870 nucleation of H_2SO_4, NH_3, and H_2O in the atmosphere, J. Geophys. Res., 104, 26,349-26,353,
871 1999.
872 Kurtén, T., Torpo, L., Ding, C.-G., Vehkamäki, H., Sundberg, M. R., Laasonen, K., and Kulmala,
873 M.: A density functional study on water-sulfuric acid-ammonia clusters and implications for at-
874 mospheric cluster formation, J. Geophys. Res., 112, D04210, doi:10.1029/2006JD007391,
875 2007.
876 Kürten, A., et al., Experimental particle formation rates spanning tropospheric sulfuric acid and
877 ammonia abundances, ion production rates, and temperatures, J. Geophys. Res. Atmos., 121,
878 12,377–12,400, doi:10.1002/2015JD023908, 2016.
879 Kürten, A., Münch, S., Rondo, L., Bianchi, F., Duplissy, J., Jokinen, T., Junninen, H., Sarnela, N.,
880 Schobesberger, S., Simon, M. and Sipilä, M., Thermodynamics of the formation of sulfuric acid

dimers in the binary (H_2SO_4–H_2O) and ternary (H_2SO_4–H_2O–NH_3) system. Atmospheric Chemistry and Physics, 15(18), pp.10701-10721, 2015.

Laakso, L., Mäkelä, J. M., Pirjola, L., and Kulmala, M., Model studies of ion-induced nucleation in the atmosphere, J. Geophys. Res., 107, 4427, doi:10.1029/2002JD002140, 2003.

Leverentz, H.R., Siepmann, J.I., Truhlar, D.G., Loukonen, V. and Vehkamäki, H., Energetics of atmospherically implicated clusters made of sulfuric acid, ammonia, and dimethyl amine, Journal of Physical Chemistry A, 117(18), 3819-3825, 2013.

Lovejoy, E. R., Curtius, J., and Froyd, K. D., Atmospheric ion-induced nucleation of sulfuric acid and water, J. Geophys. Res., 109, D08204, doi:10.1029/2003JD004460, 2004.

Ma, Y., Chen, J., Jiang, S., Liu, Y.R., Huang, T., Miao, S.K., Wang, C.Y. and Huang, W., Characterization of the nucleation precursor (H 2 SO 4–(CH 3) 2 NH) complex: intra-cluster interactions and atmospheric relevance. RSC Advances, 6(7), pp.5824-5836, 2016.

Marti, J. J., A. Jefferson, X. Ping Cai, C. Richert, P. H. McMurry, and F. Eisele, H_2SO_4 vapor pressure of sulfuric acid and ammonium sulfate solutions, J. Geophys. Res.,102(D3), 3725–3736, 1997.

McGrath, M. J., Olenius, T., Ortega, I. K., Loukonen, V., Paasonen, P., Kurtén, T., Kulmala, M., and Vehkamäki, H.: Atmospheric Cluster Dynamics Code: a flexible method for solution of the birth-death equations, Atmos. Chem. Phys., 12, 2345-2355, doi:10.5194/acp-12-2345-2012, 2012.

Meng, Z., Xu, X., Lin, W., Xie, Y., Song, B., Jia, S., Zhang, R., Peng, W., Wang, Y., Cheng, H., Yang, W., and Zhao, H., Role of ambient ammonia in particulate ammonium formation at a rural site in the North China Plain, Atmos. Chem. Phys. Discuss., https://doi.org/10.5194/acp-2017-174, in review, 2017.

Meot-Ner (Mautner), M., The Ionic Hydrogen Bond and Ion Solvation. 2. Hydration of Onium Ions by 1 - 7 H2O Molecules. Relations Between Monomolecular, Specific and Bulk Hydration, J. Am. Chem. Soc., 106, 5, 1265, 1984.

Merikanto J., I. Napari, H. Vehkamäki, T. Anttila, M. Kulmala, New parameterization of sulfuric acid-ammonia-water ternary nucleation rates at tropospheric conditions, J. Geophys. Res., 112, D15207, doi:10.1029/2006JD007977, 2007.

Miao, S.K., Jiang, S., Chen, J., Ma, Y., Zhu, Y.P., Wen, Y., Zhang, M.M. and Huang, W., Hydration of a sulfuric acid–oxalic acid complex: acid dissociation and its atmospheric implication, RSC Advances, 5(60), 48638-48646, 2015.

Nadykto, A. B., A. Al Natsheh, F. Yu, K.V. Mikkelsen, and J. Herb, Computational Quantum Chemistry: A New Approach to Atmospheric Nucleation, Advances in Quantum Chemistry, 55, 449-478, 2008.

916 Nadykto, A. B., Al Natsheh, A., Yu, F., Mikkelsen, K. V., and Ruuskanen, J., Quantum nature of
917 the sign preference in the ion-induced nucleation, Physical Review Letters, 96, 125701, 2006.
918 Nadykto, A., and Yu, F., Uptake of neutral polar vapour molecules by charged particles:
919 Enhancement due to dipole-charge interaction, J. Geophy. Res., 108(D23), 4717,
920 doi:10.1029/2003JD003664, 2003.
921 Nadykto, A.B. and Yu, F., Strong hydrogen bonding between atmospheric nucleation precursors
922 and common organics. Chemical physics letters, 435(1), pp.14-18, 2007a.
923 Nadykto, A.B., Du, H. and Yu, F., Quantum DFT and DF–DFT study of vibrational spectra of
924 sulfuric acid, sulfuric acid monohydrate, formic acid and its cyclic dimer. Vibrational
925 spectroscopy, 44(2), pp.286-296, 2007b.
926 Nadykto, A. B., F. Yu, and J. Herb,Theoretical analysis of the gas-phase hydration of common
927 atmospheric pre-nucleation $(HSO_4^-)(H_2O)_n$ and $(H_3O^+)(H_2SO_4)(H_2O)_n$ cluster ions, Chemical
928 Physics, 360, 67-73, doi:10.1016/j.chemphys.2009.04.007, 2009.
929 Nadykto, A.B., Herb, J., Yu, F. and Xu, Y., Enhancement in the production of nucleating clusters
930 due to dimethylamine and large uncertainties in the thermochemistry of amine-enhanced
931 nucleation. Chemical Physics Letters, 609, 42-49, 2014.
932 Nadykto, A.B., Herb, J., Yu, F., Nazarenko, E.S. and Xu, Y., Reply to the 'Comment on
933 "Enhancement in the production of nucleating clusters due to dimethylamine and large
934 uncertainties in the thermochemistry of amine-enhanced nucleation"'byKupiainen-Maatta et al.
935 Chemical Physics Letters, 624, 111-118, 2015.
936 Napari, I, Noppel, M, Vehkamaki, H., Kulmala, M., An improved model for ternary nucleation of
937 sulfuric acid–ammonia–water. J. Chem. Phys., 116: 4221-4227, DOI: 10.1063/1.1450557, 2002.
938 Olenius T., O. Kupiainen-Määttä, I. K. Ortega, T. Kurtén, and H. Vehkamäki, Free energy barrier
939 in the growth of sulfuric acid–ammonia and sulfuric acid–dimethylamine clusters, The Journal
940 of Chemical Physics 2013 139:8, 2013.
941 Ortega, I. K., Kupiainen, O., Kurtén, T., Olenius, T., Wilkman, O., McGrath, M. J., Loukonen, V.,
942 and Vehkamäki, H., From quantum chemical formation free energies to evaporation rates,
943 Atmos. Chem. Phys., 12, 225-235, 2012.
944 Payzant, J.D.; Cunningham, A.J.; Kebarle, P., Gas - Phase Solvation of Ammonium Ion by NH_3
945 and H_2O and Stabilities of Mixed Clusters $NH_4^+(NH_3)_n(H_2O)_w$, Can. J. Chem., 51, 19, 3242,
946 1973.
947 Peng, X.Q., Liu, Y.R., Huang, T., Jiang, S. and Huang, W., Interaction of gas phase oxalic acid
948 with ammonia and its atmospheric implications, Physical Chemistry Chemical Physics, 17(14),
949 9552-9563, 2015.
950 Raes, F., A. Janssens, and R. V. Dingenen, The role of ion-induced aerosol formation in the lower
951 atmosphere, J. Aerosol Sci., 17, 466–470, 1986.

Schnitzhofer, R., et al., Characterisation of organic contaminants in the CLOUD chamber at CERN, Atmos. Meas. Tech., 7, 2159–2168, doi:10.5194/amt-7-2159-2014, 2014.

Schobesberger, S., et al., On the composition of ammonia–sulfuric-acid ion clusters during aerosol particle formation, Atmos. Chem. Phys., 15, 55-78, https://doi.org/10.5194/acp-15-55-2015, 2015.

Sipilä, M., Berndt, T., Petäjä, T., Brus, D., Vanhanen, J., Stratmann, F., Patokoski, J., Mauldin, R. L., Hyvärinen, A. P., Lihavainen, H., and Kulmala, M.: The Role of Sulfuric Acid in Atmospheric Nucleation, Science, 327, 1243, https://doi.org/10.1126/science.1180315, 2010.

Sorokin, A., Arnold, F. and Wiedner, D., Formation and growth of sulfuric acid–water cluster ions: Experiments, modelling, and implications for ion-induced aerosol formation, Atmospheric Environment, 40, 2030-2045, 2006.

Temelso, B., Morrell, T.E., Shields, R.M., Allodi, M.A., Wood, E.K., Kirschner, K.N., Castonguay, T.C., Archer, K.A. and Shields, G.C., Quantum mechanical study of sulfuric acid hydration: Atmospheric implications. The Journal of Physical Chemistry A, 116(9), 2209-2224, 2012a.

Temelso, B., Phan, T.N. and Shields, G.C., Computational study of the hydration of sulfuric acid dimers: Implications for acid dissociation and aerosol formation, Journal of Physical Chemistry A, 116(39), pp.9745-9758, 2012b.

Thomson, J. J., Applications of Dynamics to Physics and Chemistry, 1st ed., Cambridge University Press, London,1888.

Torpo, L., Kurtén, T., Vehkamäki, H., Laasonen, K., Sundberg, M.R. and Kulmala, M., Significance of ammonia in growth of atmospheric nanoclusters. The Journal of Physical Chemistry A, 111(42), pp.10671-10674, 2007.

Vehkamäki H., Kulmala, M., Napari, I., Lehtinen, K. E. J., Timmreck, C., Noppel, M., and Laaksonen, A., An improved parameterization for sulfuric acid–water nucleation rates for tropospheric and stratospheric conditions, J. Geophys. Res., 107 (D22), 4622, doi:10.1029/2002JD002184, 2002.

Warner, J. X., Wei, Z., Strow, L. L., Dickerson, R. R., & Nowak, J. B.. The global tropospheric ammonia distribution as seen in the 13-year AIRS measurement record. Atmospheric Chemistry and Physics, 16(8), 5467-5479. https://doi.org/10.5194/acp-16-5467-2016, 2016.

Wilhelm, S., Eichkorn, S., Wiedner, D., Pirjola, L. and Arnold, F.: Ion-induced aerosol formation: new insights from laboratory measurements of mixed cluster ions, $HSO_4^-(H_2SO_4)_a(H_2O)_w$ and $H^+(H_2SO_4)_a(H_2O)_w$, Atmos. Environ., 38, 1735-1744, 2004.

Włodek, S., Z. Łuczyński, H. Wincel, Stabilities of gas-phase NO_3^- $(HNO_3)_n$, n ⩽ 6, clusters, In International Journal of Mass Spectrometry and Ion Physics, 35, 1–2, 1980, 39-46, 1980.

Xu, W. and Zhang, R., A theoretical study of hydrated molecular clusters of amines and dicarboxylic acids, Journal of chemical physics, 139(6), p.064312, 2013.

Xu, W. and Zhang, R., Theoretical investigation of interaction of dicarboxylic acids with common aerosol nucleation precursors, Journal of Physical Chemistry A, 116(18), 4539-4550, 2012.

Yu, F., and Turco, R. P., The role of ions in the formation and evolution of particles in aircraft plumes, Geophys. Res. Lett., 24, 1927-1930, 1997.

Yu, F., and Turco, R. P., Ultrafine aerosol formation via ion-mediated nucleation, Geophys. Res. Lett., 27, 883-886, 2000.

Yu, F., and R. P. Turco: From molecular clusters to nanoparticles: The role of ambient ionization in tropospheric aerosol formation, J. Geophys. Res., 106, 4797-4814, 2001.

Yu, F. and Turco, R. P., The size-dependent charge fraction of sub-3-nm particles as a key diagnostic of competitive nucleation mechanisms under atmospheric conditions, Atmos. Chem. Phys., 11, 9451–9463, doi:10.5194/acp-11-9451-2011, 2011.

Yu, F., Modified Kelvin-Thomson equation considering ion-dipole interaction: Comparison with observed ion-clustering enthalpies and entropies, J. Chem. Phys., 122, 084503, 2005.

Yu, F., Effect of ammonia on new particle formation: A kinetic H_2SO_4-H_2O-NH_3 nucleation model constrained by laboratory measurements, J. Geophys. Res., 111, D01204, doi:10.1029/2005JD005968, 2006a.

Yu, F., From molecular clusters to nanoparticles: Second-generation ion-mediated nucleation model, Atmos. Chem. Phys., 6, 5193-5211, 2006b.

Yu, F., Improved quasi-unary nucleation model for binary H_2SO_4-H_2O homogeneous nucleation, J. Chem. Phys., 127, 054301, 2007.

Zhang, R, Khalizov, AF, Wang, L, Hu,M, Wen,X., Nucleation and growth of nanoparticles in the atmosphere, Chem. Rev. 112: 1957-2011, DOI: 10.1021/cr2001756, 2012.

Zhang, R., Wang, L., Khalizov, A.F., Zhao, J., Zheng, J., McGraw, R.L. and Molina, L.T., Formation of nanoparticles of blue haze enhanced by anthropogenic pollution, Proceedings of the National Academy of Sciences, 106(42), 17650-17654, 2009.

Zhang, Y., P. H. McMurry, F. Yu, and M. Z. Jacobson, A Comparative Study of Homogeneous Nucleation Parameterizations, Part I. Examination and Evaluation of the Formulations, J. Geophys. Res., 115, D20212, doi:10.1029/2010JD014150, 2010.

Zhu, Y.P., Liu, Y.R., Huang, T., Jiang, S., Xu, K.M., Wen, H., Zhang, W.J. and Huang, W., Theoretical study of the hydration of atmospheric nucleation precursors with acetic acid, Journal of Physical Chemistry A, 118(36), 7959-7974, 2014.

1021 Zollner, J. H., W. A. Glasoe, B. Panta, K. K. Carlson, P. H. McMurry, and D. R. Hanson, Sulfuric
1022 acid nucleation: Power dependencies, variation with relative humidity, and effect of bases,
1023 Atmos. Chem. Phys., 12(10), 4399–4411, doi:10.5194/acp-12-4399-2012, 2012.
1024

Table A1. Number of isomers successfully converged at 6-311 level for selected clusters, along with the enthalpy, entropy, and Gibbs free energy of the most stable isomers.

Cluster Formula	6-311++ conv.	Enthalpy (Hartree)	Entropy (cal/K·mol)	Gibbs free energy (Hartree)
S_4	56	-2801.256008	179.461	-2801.341276
S_4A_1	169	-2857.820795	187.395	-2857.909833
S_4A_2	84	-2914.388489	193.997	-2914.480663
S_4A_3	68	-2970.94645	209.77	-2971.046119
S_4A_4	38	-3027.500303	225.959	-3027.607663
S_4A_5	34	-3084.050337	237.758	-3084.163303
S^-S_3	97	-2800.835072	168.993	-2800.915366
$S^-S_3A_1$	122	-2857.389946	184.899	-2857.477797
$S^-S_3A_2$	21	-2913.941409	192.489	-2914.032867
$S^-S_3A_3$	13	-2970.490814	195.627	-2970.583762
S^-S_4	138	-3501.162655	200.525	-3501.257931
$S^-S_4A_1$	71	-3557.727072	208.015	-3557.825907
$S^-S_4A_2$	22	-3614.287482	213.397	-3614.388874
$S^-S_4A_3$	23	-3670.836831	226.504	-3670.94445
$S^-S_4A_4$	18	-3727.385956	237.152	-3727.498634
H^+A_2	16	-113.413269	68.478	-113.445805
$H^+A_2W_1$	42	-189.845603	94.248	-189.890384
$H^+A_2W_2$	56	-266.276653	113.49	-266.330576
$H^+A_2W_3$	63	-342.706301	132.722	-342.769362
$H^+A_2W_4$	114	-419.133157	160.449	-419.209391
$H^+A_2W_5$	116	-495.567408	161.447	-495.644117
$H^+A_2W_6$	70	-571.994961	175.085	-572.078149
$H^+A_2W_0S_1$	40	-813.745253	107.764	-813.796455
$H^+A_2W_1S_1$	173	-890.181285	121.33	-890.238933
$H^+A_2W_2S_1$	103	-966.618165	130.584	-966.680209
$H^+A_2W_3S_1$	169	-1043.047622	154.145	-1043.120861
$H^+A_2W_4S_1$	188	-1119.476882	177.051	-1119.561004
$H^+A_2W_5S_1$	178	-1195.90253	200.029	-1195.99757
$H^+A_2W_6S_1$	85	-1272.330781	215.117	-1272.43299

Table A2. QC-based stepwise Gibbs free energy change (in kcal/mol) for the addition of one water (ΔG^{o}_{+W}), ammonia (ΔG^{o}_{+A}), or sulfuric acid (ΔG^{o}_{+S}) molecule to form the given positively charged clusters under standard conditions, and the corresponding experimental data or semi-experimental estimates.

	ΔG^{o}_{+W}		ΔG^{o}_{+A}		ΔG^{o}_{+S}	
	QC	experimental	QC	experimental	QC	experimental
$H^+W_1S_1$					-28.59	-24.65 [f]
$H^+W_2S_1$	-15.66				-15.33	-13.76 [f]
$H^+W_3S_1$	-9.40				-10.12	-11.93 [f]
$H^+W_4S_1$	-7.83				-9.18	-9.71 [f]
$H^+W_5S_1$	-6.77	-5.79 [a]			-9.52	-9.82 [f]
$H^+W_6S_1$	-5.32	-4.24 [a]			-9.70	-9.94 [f]
$H^+W_7S_1$	-3.18	-3.28 [a]			-9.64	-9.96 [f]
$H^+W_8S_1$	-2.80	-2.67 [a]			-9.84	-10.10 [f]
$H^+W_9S_1$	-2.30	-2.12 [a]			-10.24	-10.86 [f]
$H^+A_1W_1$	-13.47	-13.01 [b], -11.43 [c]	-52.08			
$H^+A_1W_2$	-9.85	-7.14 [b], -8.17 [c]	-33.02			
$H^+A_1W_3$	-6.60	-5.92 [b], -5.88 [c]	-25.01			
$H^+A_1W_4$	-3.50	-3.94 [b], -4.06 [c]	-19.73			
$H^+A_1W_5$	-2.50	-2.55 [b],-3.02 [c]	-15.80			
$H^+A_1W_6$	-2.26	-2.54 [b]	-12.93			
$H^+A_1W_7$	-1.15	-1.84 [b]	-10.84			
$H^+A_1W_8$	-1.02		-9.26			
$H^+A_1W_9$	0.25		-8.32			
H^+A_2			-22.97	-18.25 [c]		
$H^+A_2W_1$	-7.04	-6.85 [c]	-16.53	-11.54 [c], -12.75 [d]		
$H^+A_2W_2$	-4.29	-5.25 [c]	-10.97	-9.13 [c], -9.50 [d]		
$H^+A_2W_3$	-3.41	-3.70 [c]	-7.78	-6.83 [c], -7.02 [d]		
$H^+A_2W_4$	-3.08		-7.36			
$H^+A_2W_5$	-1.97		-6.82			
$H^+A_2W_6$	-0.42		-4.99			
$H^+A_1W_1S_1$	-8.99		-33.14		-9.65	-8.3 [d]
$H^+A_1W_2S_1$	-8.11		-25.59		-7.90	-7.1 [d]
$H^+A_1W_3S_1$	-6.09		-22.28		-7.40	-6.7 [d]
$H^+A_1W_4S_1$	-4.25		-18.71		-8.15	-6.9 [d]
$H^+A_1W_5S_1$	-1.92		-13.85		-7.56	-7.5 [d]
$H^+A_1W_6S_1$	-2.04		-10.57		-7.34	-8.0 [d]
$H^+A_2W_0S_1$			-22.09	-22.14 [e]	-13.35	-16.8 [d]

$H^+A_2W_1S_1$	-5.72	-18.92	-12.03	-15.8 [d]
$H^+A_2W_2S_1$	-4.97	-15.78	-12.71	-15.9 [d]
$H^+A_2W_3S_1$	-4.58	-14.27	-13.89	-16.3 [d]
$H^+A_2W_4S_1$	-4.26	-14.27	-15.06	-17.3 [d]
$H^+A_2W_5S_1$	-2.01	-14.37	-15.11	-18.8 [d]
$H^+A_2W_6S_1$	-1.29	-13.63	-15.98	-19.9 [d]

[a] Froyd and Lovejoy, 2003; [b] Meot-Ner (Mautner) et al., 1984; [c] Payzant et al., 1973; [d] Froyd, 2002; [e] Froyd and Lovejoy, 2012. [f] The ΔG^o_{+S} values given here were calculated based on experimental ΔG^o_{+S} values at T=270 K from Froyd and Lovejoy (2003) and ΔS values from quantum calculation.

Table A3. Same as Table A2 except for neutral clusters.

	ΔG^{o}_{+W}		ΔG^{o}_{+A}		ΔG^{o}_{+S}	
	QC	experimental	QC	experimental	QC	experimental
S_1A_1			-7.77 [a] (-7.29 [b], -7.61 [c], -6.60 [d])	- 8.2 [e]	-7.77 [a] (-7.29 [b], -7.61 [c], -6.60 [d])	- 8.2 [e]
$S_1A_1W_1$	-1.39 [a]		-6.88 [a]			
$S_1A_1W_2$	-2.30 [a]		-6.18 [a]			
$S_1A_1W_3$	-1.52 [a]		-5.81 [a]			
S_1A_2			-4.75			
$S_1A_2W_1$	-0.78		-4.15			
S_2A_1			-13.84 [a]		-11.65 [a]	
$S_2A_1W_1$	-2.31 [a]		-12.77		-12.59 [a]	
$S_2A_1W_2$	-1.21 [a]		-11.00		-11.52 [a]	
$S_2A_1W_3$	-2.04 [a]		-9.69		-12.04 [a]	
S_2A_2			-8.75		-15.65	
$S_2A_2W_1$	-1.96		-8.37		-16.83	
$S_2A_2W_2$	-1.19		-8.35		-15.49	
$S_2A_2W_3$	0.60		-5.71		-14.42	
S_2A_3			-4.19			
S_3A_1			-16.14		-7.08	
S_3A_2			-13.84		-12.17	
S_3A_3			-8.93		-16.92	
S_3A_4			-7.42			
S_4A_1			-15.74		-4.16	
S_4A_2			-17.16		-7.48	
S_4A_3			-13.79		-12.34	
S_4A_4			-11.34		-16.26	
S_4A_5			-7.63			

[a] Nadykto and Yu, 2007; [b] Torpo et al., 2007; [c] Ortega et al., 2012; [d] Chon et al., 2007; [e] Kurten et al., 2015.

Table A4. Same as Table A2 except for negatively charged clusters.

	ΔG^{o}_{+W}		ΔG^{o}_{+A}		ΔG^{o}_{+S}	
	QC	experimental	QC	experimental	QC	experimental
$S^- A_1$			2.81			
$S^- S_1W_0$					-32.74	-29.10[a]
$S^- S_1W_1$	-0.61				-28.12	
$S^- S_1W_2$	-1.06				-25.36	
$S^- S_1A_1$			0.08		-35.47	
$S^- S_2W_0$					-15.06	-17.14[a]
$S^- S_2W_1$	-1.83				-16.28	
$S^- S_2A_1$			-4.85		-19.99	
$S^- S_3W_0$					-10.58	-13.28 [a]
$S^- S_3W_1$	-2.92	-2.73 [a]			-11.67	-14.29 [a]
$S^- S_3W_2$	-2.03	-1.53 [a]			-11.12	-13.80 [a]
$S^- S_3W_3$	-2.01	-1.93 [a]			-11.52	-14.72 [a]
$S^- S_3W_4$	-1.73					
$S^- S_3A_1W_0$			-11.89		-17.62	
$S^- S_3A_1W_1$	0.52		-8.45		-14.90	
$S^- S_3A_1W_2$	0.39		-6.03		-13.06	
$S^- S_3A_2$			-7.27		-18.36	
$S^- S_3A_3$			-4.66			
$S^- S_4W_0$					-8.28	-10.96 [a]
$S^- S_4W_1$	-3.50	-2.61 [a]			-8.86	-10.71 [a]
$S^- S_4W_2$	-3.17	-2.79 [a]			-9.99	-12.10 [a]
$S^- S_4W_3$	-2.65	-2.41 [a]			-10.64	-12.48 [a]
$S^- S_4W_4$	-2.25	-2.14 [a]			-11.16	-12.77 [a]
$S^- S_4A_1W_0$			-15.37		-11.76	
$S^- S_4A_1W_1$	-2.21		-14.09		-14.49	
$S^- S_4A_1W_2$	-0.74		-11.66		-15.62	
$S^- S_4A_2$			-12.23		-16.71	
$S^- S_4A_3$			-7.59		-19.65	
$S^- S_4A_4$			-6.72			

[a] Froyd and Lovejoy, 2003.

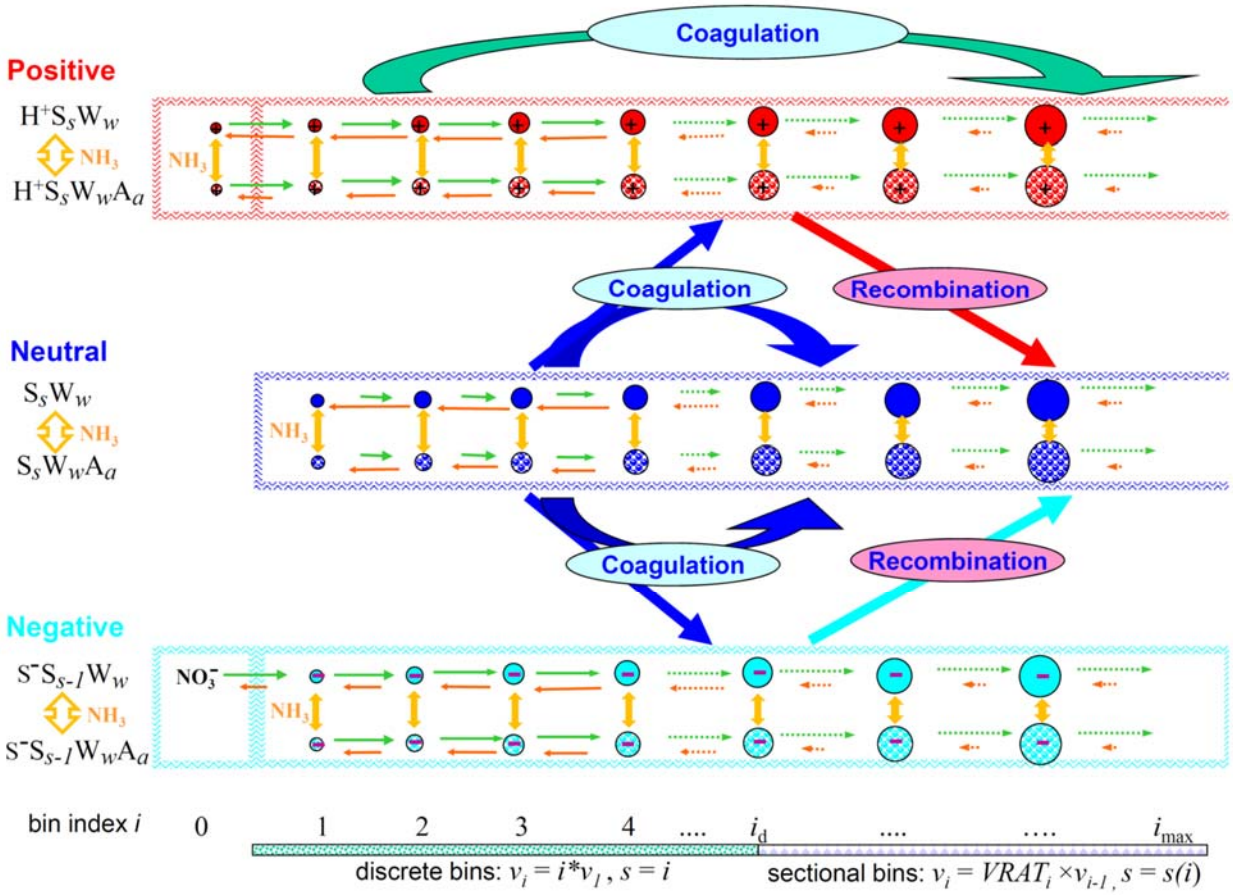

Figure 1. Schematic illustration of kinetic processes controlling the evolution of positively charged ($H^+S_sW_wA_a$), neutral ($S_sW_wA_a$), and negatively charged ($S^-S_{s-1}W_wA_a$) clusters/droplets that are explicitly simulated in the ternary ion-mediated nucleation (TIMN) model. Here S, W, and A represent sulfuric acid (H_2SO_4), water (H_2O), and ammonia (NH_3) respectively, while *s*, *w*, and *a* refer to the number of S, W, and A molecules in the clusters/droplets, respectively. The TIMN model has been extended from an earlier version treating binary IMN (BIMN) by adding NH_3 into the nucleation system and using a discrete-sectional bin structure to represent the sizes of clusters/particles starting from a single molecule up to background particles larger than a few micrometers.

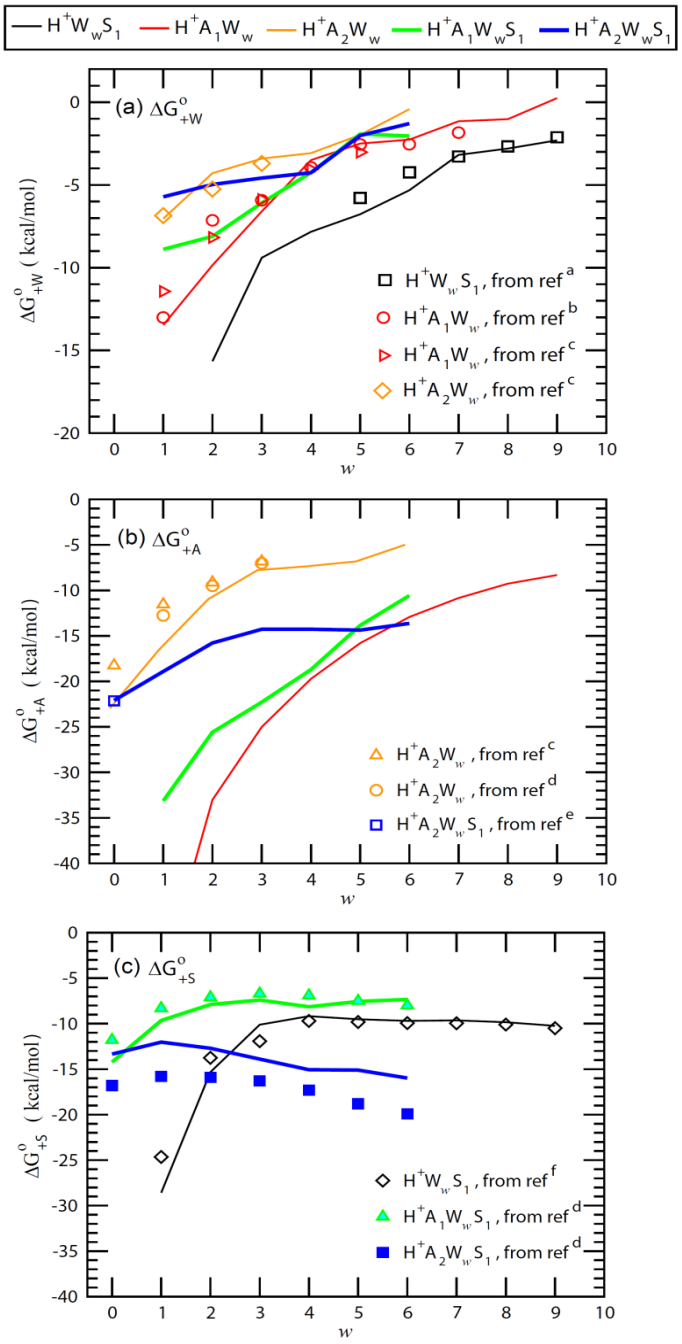

Figure 2. Stepwise Gibbs free energy change under standard conditions for the addition of a water (ΔG^{o}_{+W}), ammonia (ΔG^{o}_{+A}), or sulfuric acid (ΔG^{o}_{+S}) molecule to form the given positively charged clusters as a function of the number of water molecules in the clusters (*w*). Lines are QC-based values, and symbols are experimental results or semi-experimental estimates (see notes under Table A2 for the references).

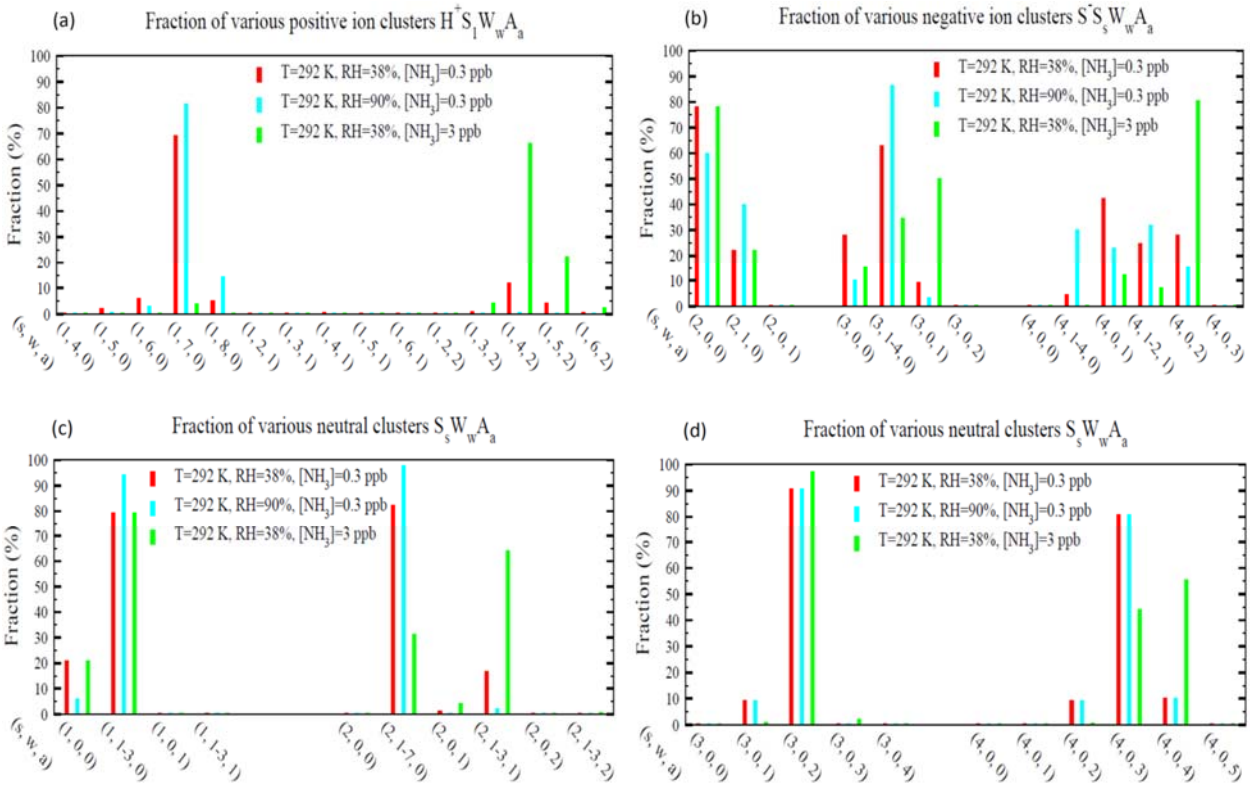

Figure 3. Relative abundance (or molar fraction) of small clusters containing a given number of H_2SO_4 molecules for positive, negative, and neutral cluster types at a temperature of 292 K and three different combinations of RHs (38% and 90%) and [NH_3] (0.3 and 3 ppb). Some clusters with different numbers of water molecules were grouped together to make the plot more clear and neat. For the clusters shown in panel (d), there is no hydrate data and thus hydration for these clusters were not calculated.

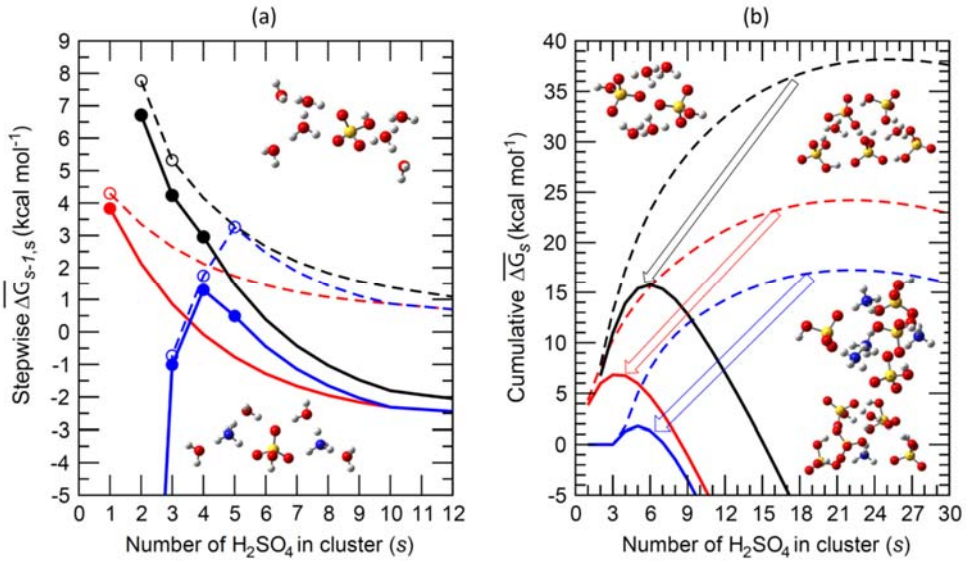

Figure 4. (a) Average stepwise Gibbs free energy change for the addition of one H_2SO_4 molecule to form a neutral (black), positively charged (red), or negatively charged (blue) binary H_2SO_4-H_2O (dashed lines or empty circles) or ternary H_2SO_4-H_2O-NH_3 (solid lines or filled circles) cluster containing s H_2SO_4 molecules ($\overline{\Delta G}_{s-1,s}$); (b) Same as (a) but for the cumulative (total) Gibbs free energy change in each case. Filled and empty circles in (a) refer to $\overline{\Delta G}_{s-1,s}$ obtained using measurements and/or quantum-chemical calculations. $\overline{\Delta G}_{s-1,s}$ for larger clusters with $s \geq 10$, which approach the properties of the equivalent bulk liquid (20), are calculated using the capillarity approximation. Interpolation is used to calculate $\overline{\Delta G}_{s-1,s}$ for clusters up to s=10 (Eq. 11). Calculations were carried out at T=292 K, RH=38%, $[H_2SO_4]=3\times10^8$ cm^{-3} and $[NH_3]$= 0.3 ppb. The inset diagrams represent equilibrium geometries for the most stable isomers of selected binary clusters ($(H_3O^+)(H_2SO_4)(H_2O)_6$, $(H_2SO_4)_2(H_2O)_4$, and $(HSO_4^-)(H_2SO_4)_4(H_2O)_2$), and ternary clusters ($(NH_4^+)(H_2SO_4)(NH_3)(H_2O)_4$, $(HSO_4^-)(H_2SO_4)_4(H_2O)(NH_3)$, $(H_2SO_4)_4(NH_3)_4$).

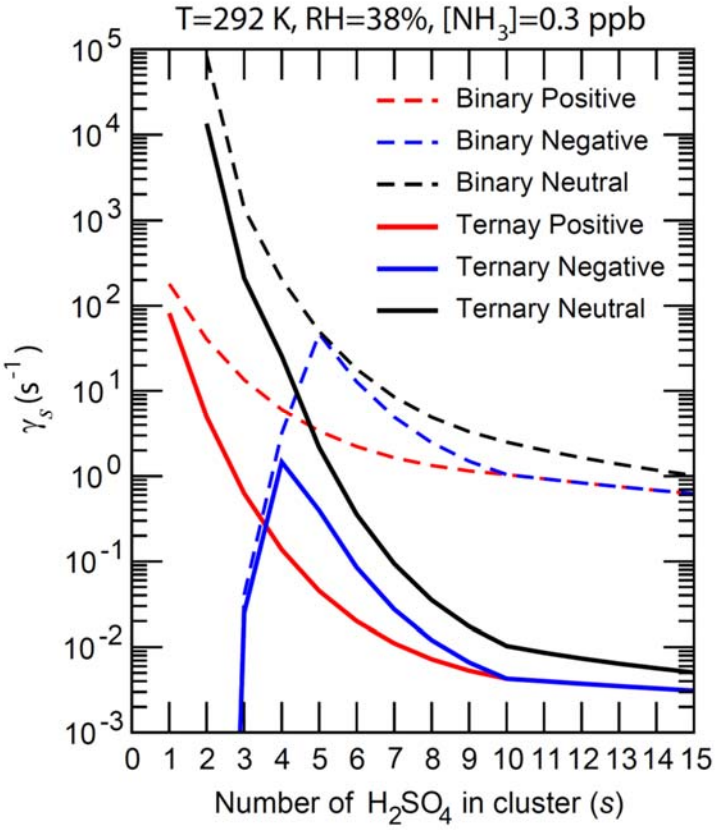

1090

1091 **Figure 5.** The number-concentration-weighted mean evaporation rates ($\bar{\gamma}$) of H_2SO_4 molecules
1092 from neutral clusters (black), positively charged clusters (red), and negatively charged clusters
1093 (blue) for binary (H_2SO_4-H_2O, dashed lines) and ternary (H_2SO_4-H_2O-NH_3, solid lines) nucleating
1094 systems containing s H_2SO_4 molecules ($\overline{\Delta G}_{s-1,s}$). T=292 K, RH=38%, and [NH_3] = 0.3 ppb for
1095 the ternary system.

1096

1097

1098

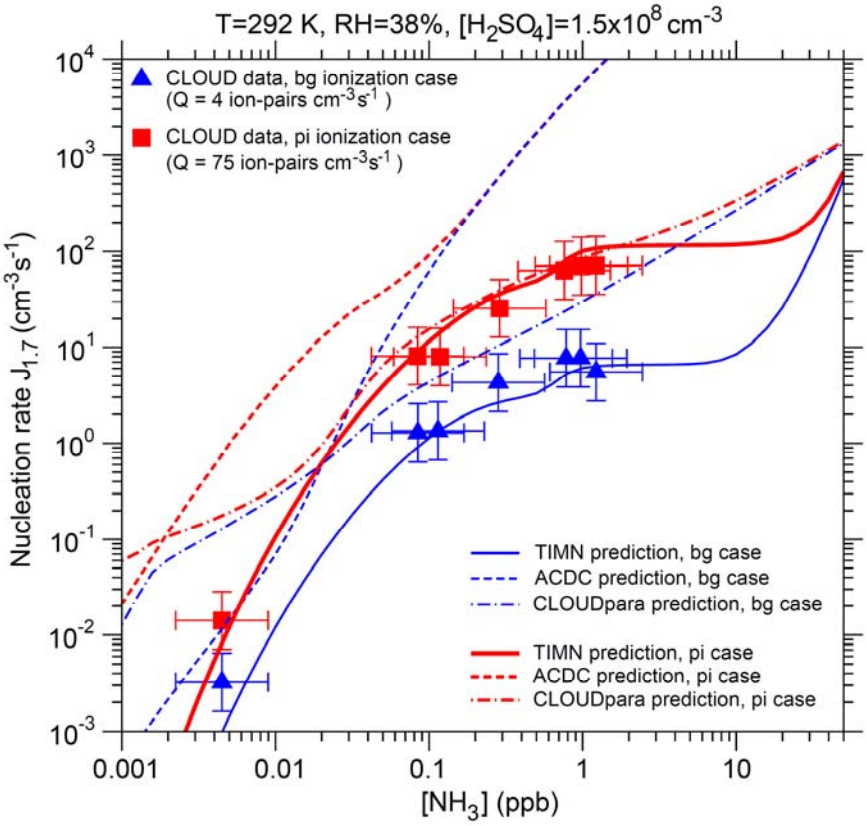

Figure 6. Effect of ammonia concentrations ([NH_3]) on effective nucleation rates calculated at a cluster mobility diameter of 1.7 nm ($J_{1.7}$, lines) under the stated conditions with two ionization rates (Q) – background ionization, bg (blue), and ionization enhanced by a pion beam, pi (red). Also shown are predictions from the TIMN model, the Atmospheric Cluster Dynamics Code (ACDC) with thermochemistry obtained using RI-CC2//B3LYP method (McGrath et al., 2012; Kurten et al., 2016), and an empirical parameterization of CLOUD measurements (CLOUDpara) (Dunne et al., 2016) are indicated by solid, dashed, and dot-dashed lines, respectively. The symbols refer to CLOUD experimental data (Kirkby et al., 2011; Dunne et al., 2016), with the uncertainties in measured [NH_3] and $J_{1.7}$ shown by horizontal and vertical bars, respectively. To be comparable, the CLOUD data points given in Dunne et al. (2016) under the conditions of T=292 K and RH=38% with [H_2SO_4] close to 1.5×10^8 cm^{-3} have been interpolated to the same [H_2SO_4] value ($=1.5\times10^8$ cm^{-3}).

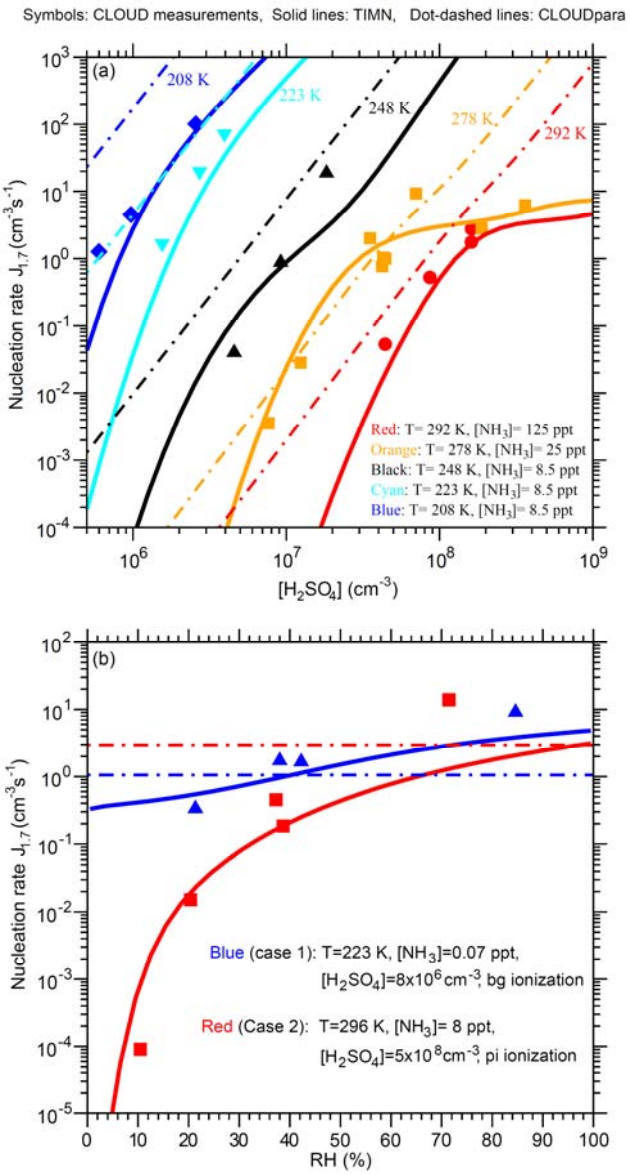

Figure 7. Comparison of TIMN simulations (solid lines), CLOUDpara predictions (Dunne et al., 2016) (dot-dashed lines) and CLOUD measurements (symbols, data from Dunne et al. (2016) of the dependences of nucleation rates on (a) $[H_2SO_4]$ at five different temperatures (T=292, 278, 248, 223, and 208 K) and (b) RH at two sets of conditions as specified. $[NH_3]$ is in ppt (parts per trillion, by volume). Error bars for the uncertainties in measured $[H_2SO_4]$ (-50%, +100%), $[NH_3]$ (-50%, +100%), and $J_{1.7}$ (overall a factor of two) are not shown. To be comparable, the CLOUD data points given in Dunne et al. (2016) under the conditions (T, RH, ionization rate) with $[NH_3]$ or $[H_2SO_4]$ close to the corresponding values specified in the figure legends have been interpolated to the same $[NH_3]$ (Fig. 7a) or $[H_2SO_4]$ (Fig. 7b) values.

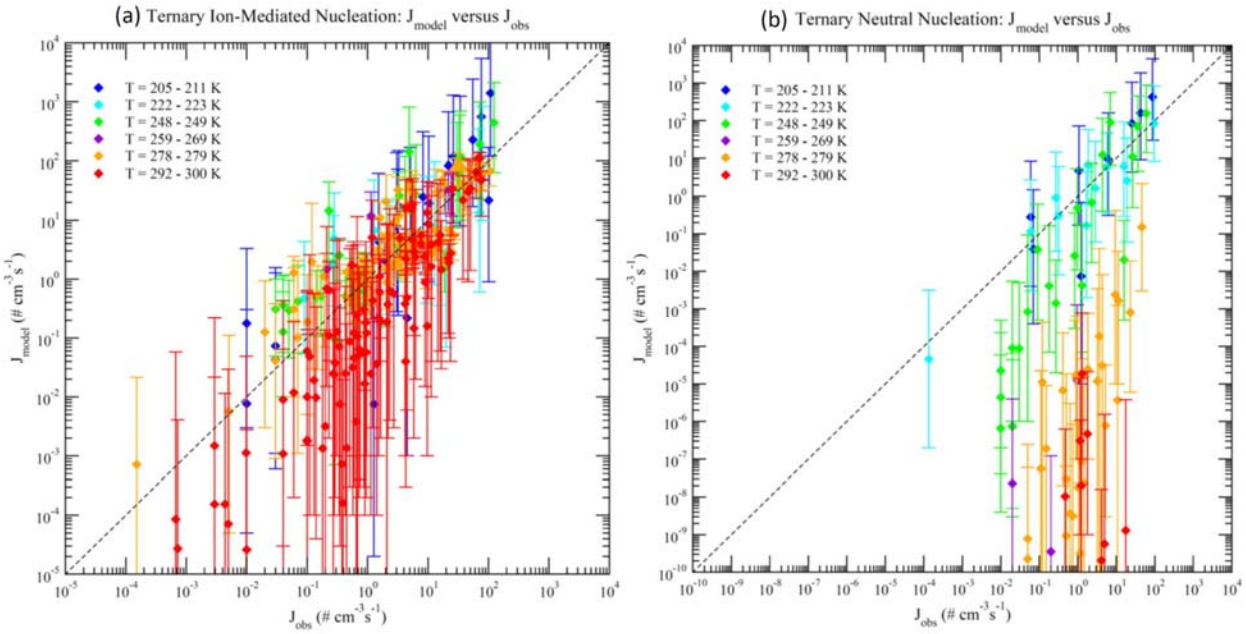

Figure 8. Model predicted (J_{model}) versus observed (J_{obs}) nucleation rates under various conditions of all 377 data points of CLOUD measurements reported in Table S1 of Dunne et al. (2016), with (a) and without (b) the presence of ionization. The data points are grouped according to temperatures as specified in the legend. Vertical error bars show the range of J_{model} calculated at 50% and 200% of measured [H_2SO_4], corresponding to the uncertainties in measured [H_2SO_4] (-50%, +100%). Error bars associated with the uncertainties in measured [NH_3] (-50%, +100%), and J_{obs} (overall a factor of two) are not shown.